Article

Cell Reports

Aberrant Calcium Signaling in Astrocytes Inhibits Neuronal Excitability in a Human Down Syndrome Stem Cell Model

Graphical Abstract

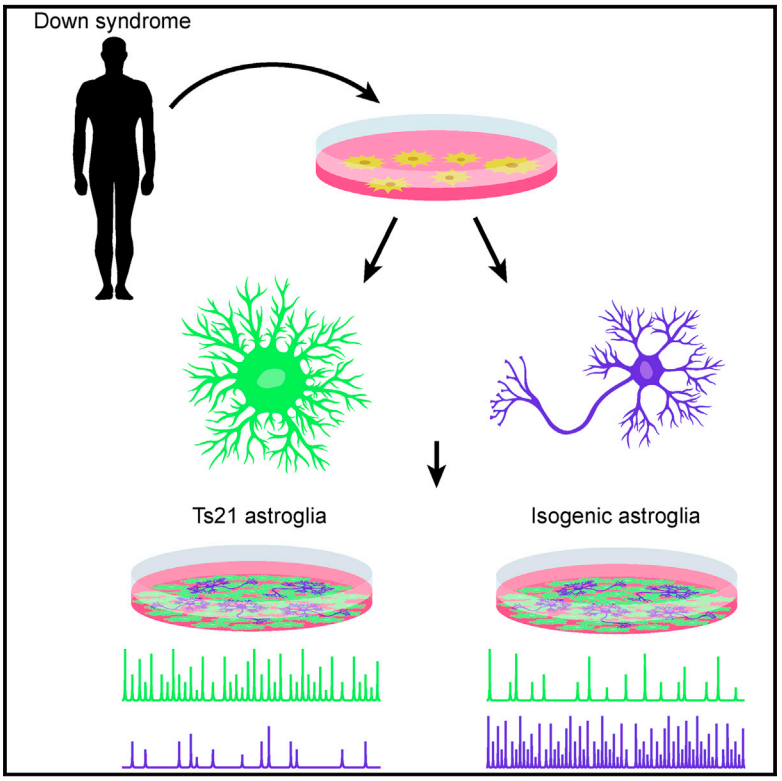

Authors

Grace O. Mizuno, Yinxue Wang, Guilai Shi, ..., Guoqiang Yu, Loren L. Looger, Lin Tian

Correspondence

lintian@ucdavis.edu

In Brief

To understand how Down syndrome (DS) affects neural networks, Mizuno et al. used a DS-patient-derived stem cell model and calcium imaging to investigate the functional defects of DS astrocytes and their effects on neuronal excitability. Their study reveals that DS astroglia exhibited more frequent spontaneous calcium fluctuations, which impair neuronal excitability.

Highlights

- Neuron-astrocyte interactions in a human DS stem cell model
- DS astroglia exhibited more frequent spontaneous Ca^{2+} fluctuations
- Spontaneous DS astroglia Ca^{2+} reduced excitability of co-cultured neurons
- Abolishing astrocytic spontaneous Ca^{2+} rescued suppressed neuronal activity

Mizuno et al., 2018, Cell Reports *24*, 355–365
July 10, 2018
https://doi.org/10.1016/j.celrep.2018.06.033

CellPress

Cell Reports
Article

Aberrant Calcium Signaling in Astrocytes Inhibits Neuronal Excitability in a Human Down Syndrome Stem Cell Model

Grace O. Mizuno,[1,8] Yinxue Wang,[3,8] Guilai Shi,[1,8] Yizhi Wang,[3] Junqing Sun,[2] Stelios Papadopoulos,[1] Gerard J. Broussard,[1] Elizabeth K. Unger,[1] Wenbin Deng,[7] Jason Weick,[5] Anita Bhattacharyya,[4] Chao-Yin Chen,[2] Guoqiang Yu,[3] Loren L. Looger,[6] and Lin Tian[1,9,*]

[1]Department of Biochemistry and Molecular Medicine, Department of Psychiatry and Behavioral Sciences, University of California, Davis, Davis, CA, USA
[2]Department of Pharmacology, University of California, Davis, Davis, CA, USA
[3]Bradley Department of Electrical and Computer Engineering, Virginia Polytechnic Institute and State University, Blacksburg, VA, USA
[4]Waisman Center, University of Wisconsin, Madison, Madison, WI, USA
[5]Department of Neuroscience, University of New Mexico, Albuquerque, NM, USA
[6]Janelia Research Campus, Howard Hughes Medical Institute, Ashburn, VA, USA
[7]Department of Biochemistry and Molecular Medicine, Shriner's Hospital, University of California, Davis, Davis, CA, USA
[8]These authors contributed equally
[9]Lead Contact
*Correspondence: lintian@ucdavis.edu
https://doi.org/10.1016/j.celrep.2018.06.033

SUMMARY

Down syndrome (DS) is a genetic disorder that causes cognitive impairment. The staggering effects associated with an extra copy of human chromosome 21 (HSA21) complicates mechanistic understanding of DS pathophysiology. We examined the neuron-astrocyte interplay in a fully recapitulated HSA21 trisomy cellular model differentiated from DS-patient-derived induced pluripotent stem cells (iPSCs). By combining calcium imaging with genetic approaches, we discovered the functional defects of DS astroglia and their effects on neuronal excitability. Compared with control isogenic astroglia, DS astroglia exhibited more-frequent spontaneous calcium fluctuations, which reduced the excitability of co-cultured neurons. Furthermore, suppressed neuronal activity could be rescued by abolishing astrocytic spontaneous calcium activity either chemically by blocking adenosine-mediated signaling or genetically by knockdown of inositol triphosphate (IP_3) receptors or S100B, a calcium binding protein coded on HSA21. Our results suggest a mechanism by which DS alters the function of astrocytes, which subsequently disturbs neuronal excitability.

INTRODUCTION

Down syndrome (DS) is a neurodevelopmental disorder occurring in 1 in 750 live births worldwide. DS is caused by trisomy of chromosome 21 (Ts21) (Dierssen, 2012), leading to triplication of up to 400 genes, resulting in an array of phenotypes, including profoundly impaired cognitive function. The brains of DS patients demonstrate consistent pathophysiological changes, such as reduced volume, altered neuronal densities and structure, and disturbed balance of all cell types. Confronted with this genetic complexity, it is difficult to determine precise molecular and cellular mechanisms of disease establishment and maintenance. Consequently, there are no therapeutic approaches to mitigate the effects of DS.

To date, DS pathophysiology has been primarily studied in rodent models (Ts65Dn, Ts1cje, and Ts1Rhr; Das and Reeves, 2011). Though useful information has been revealed, rodent models do not faithfully reproduce DS pathophysiology, due in part to incomplete synteny between HSA21 and homologous mouse regions. Furthermore, rodent modeling of complex neurodevelopmental disorders, such as DS, is limited by the fact that the human brain is far more complicated than the rodent brain in terms of structure of the neural circuitry, plasticity, and cognitive capacity.

Advances in induced pluripotent stem cell (iPSC) technology have enabled the modeling of complex diseases, such as DS in the context of human cell biology (Chen et al., 2014; Murray et al., 2015; Weick et al., 2013). These models are highly desirable for understanding disease neuropathophysiology and for developing therapeutics. By culturing iPSCs from DS individuals, it is possible to achieve full expression of the human HSA21 region. In addition, the use of isogenic control lines eliminates inter-individual variability, restricting genotype differences solely to HSA21 dosage.

Recent studies using Ts21-iPSC-derived DS models have revealed deficits in human neurons or astroglia associated with DS (Chen et al., 2014; Huo et al., 2018; Murray et al., 2015; Shi et al., 2012). Weick et al. (2013) established Ts21-iPSC lines from two sets of human fibroblasts and differentiated them into neurons. They found that Ts21-cortical neurons displayed reduced synaptic activity compared to control neurons, while maintaining the

ratio of differentiated excitatory and inhibitory neurons. Furthermore, a recent follow-up study using similar model reported impaired migration of DS inhibitory neurons (Huo et al., 2018). Chen et al. (2014), on the other hand, engineered Ts21 iPSCs from a different human fibroblast line and reported that conditioned medium from Ts21-iPSC-derived astroglia had a toxic effect on neuronal maturation and survival.

However, these studies only focus on morphological view of differentiated cells and examined neurons and astrocytes in isolation. Growing evidence suggests that astrocytes substantially contribute to neurological and psychiatric disorders by affecting neuronal function (Cao et al., 2013; Di Giorgio et al., 2008; Marchetto et al., 2008; Molofsky et al., 2012; Tong et al., 2014). Indeed, astrocytes have been implicated in multiple rodent studies as playing an important role in DS (Ballestín et al., 2014; Bambrick et al., 2003). A number of genes involved in DS, including *THBS1* and *APP*, have been shown to be expressed in astrocytes and have been implicated in Alzheimer's disease (Garcia et al., 2010; Torres et al., 2018). A complete mechanistic understanding of DS pathophysiology requires studying the communication between neurons and astrocytes at the network level.

Unlike neurons, whose excitable membranes allow action potentials to be transmitted cell-wide within milliseconds, astrocyte-wide signaling occurs via intracellular calcium (Ca^{2+}) transients lasting for seconds (Khakh and McCarthy, 2015). These intracellular Ca^{2+} transients can be triggered by neuronal activity (Wang et al., 2006) and are thought to induce release of gliotransmitters (Angulo et al., 2004; Lee et al., 2010; Mothet et al., 2005; Newman, 2001), which in turn modulate neural activity. Although gliotransmitter identity and release mechanisms are controversial (Ota et al., 2013; Sloan and Barres, 2014; Wolosker et al., 2016), intracellular Ca^{2+} dynamics are generally acknowledged to encode astrocyte activity. More importantly, altered astrocyte calcium dynamics were reported in cultured cells from the rodent DS models (Busciglio et al., 2002; Garcia et al., 2010).

Based on these previous studies, we hypothesized that DS could affect neuronal excitability through altered astrocytic Ca^{2+} dynamics, leading to alterations in astrocyte-neuron signaling pathways. Therefore, we differentiated the Ts21-iPSC lines reported in Weick et al. (2013) to astrocytes and neurons to establish a Ts21-iPSC-derived neuron-astrocyte co-culturing system to uncover functional deficits of neural networks. We focused on astrocytic Ca^{2+} dynamics and the specific interactions between astrocytes and neurons.

RESULTS

Generation and Differentiation of Astroglia from Human Ts21 iPSCs

Using established protocols (Krencik et al., 2011), we differentiated astroglia from previously reported iPSC lines by Weick et al. (2013), DS1 and DS4, which are trisomic for chromosome 21, and DS2U, a control isogenic line (Figures S1A and S1B). After 120 days, all three iPSC lines robustly expressed *CD44*, *GFAP*, and *AQP4* (Figures S1D–S1F; Table S1). Karyotype analysis prior to and after experiments confirmed trisomy of DS1- and DS4-derived astroglia (DS1A and DS4A) and disomy of DS2U-induced astroglia (DS2UA) (Figure S1B). Using qRT-PCR, we further observed global expression of a panel of astrocyte-specific markers, such as *EAAT1*, *ALDOC*, *CX43*, *SOX9*, and *NFIA*, in all three lines (Figure S1C; Table S1; Molofsky et al., 2012), indicating successful astroglia differentiation of the iPSCs. Consistent with previous reports, DS astroglia showed increased expression levels of HSA21 genes compared to control astroglia, including *S100B* (Esposito et al., 2008), *APP* (Busciglio et al., 2002), and *ETS2* (Wolvetang et al., 2003), as well as higher levels of non-HSA21 genes associated with oxidative stress, such as *CAT* (Busciglio and Yankner, 1995) and *CRYZ* (Weick et al., 2013; Figure S1C; Table S1). Morphologically, DS astroglia occupied larger territories than DS2UA; the total arborization size of DS astrocytes was significantly greater than that of control isogenic astroglia (Figure S1G).

DS Astroglia Inhibit the Excitability of Co-cultured Neurons

We next studied the potential influence of DS astroglia on co-cultured neurons. Using established protocols (Chambers et al., 2009; Zhang et al., 2001), three lines of cortical $TUJ1^+$ neurons were differentiated from the DS1 and DS2U iPSC lines and a control H9 human embryonic stem cell (hESC) line (Figures S2A and S2B). Differentiated neurons were infected with lentivirus encoding *synapsin-1*-GCaMP6m (Figure S2D). To establish a baseline of neuronal excitability, we monitored fluorescence changes in neurons in response to a series of electrically evoked field potentials (FPs) in the absence of astrocytes. The magnitude of evoked Ca^{2+} transients in neurons increased with the number of applied FPs (Figure 1A). Evoked signals were abolished by addition of 1 μM tetrodotoxin (TTX) (Figure 1A), suggesting that Ca^{2+} signals in neurons were triggered by action potentials. The expression of multiple voltage-gated sodium-channel isoforms in differentiated neurons was confirmed by qRT-PCR (Figure S2E).

After confirming the basis of neuronal excitability, we recorded neuronal activity when co-cultured with DS1-, DS4-, or DS2U-derived astroglia, as well as human primary astrocytes (HA) (Figure S2C). H9 hESC-derived neurons co-cultured with DS astroglia (DS1A or DS4A) showed significantly decreased FP-evoked Ca^{2+} amplitudes relative to neurons cultured alone (normalized $\Delta F/F$; DS1A: 0.63 ± 0.06, $p < 0.01$; DS4A: 0.57 ± 0.05, $p < 0.001$), whereas neurons co-cultured with control isogenic astrocytes (DSU2A) or human primary astrocytes were not significantly affected (DS2UA: 1.00 ± 0.04, $p = 0.93$; HA: 0.88 ± 0.04, $p = 0.059$; Figure 1B).

Similar neuronal-activity suppression imposed by DS astroglia was also observed in neurons derived from the two other iPSC lines. DS2U-derived neurons co-cultured with DS astroglia (DS1A or DS4A) showed significantly decreased FP-evoked Ca^{2+} amplitudes relative to neurons cultured alone (normalized $\Delta F/F$; DS1A: 0.57 ± 0.04, $p < 0.001$; DS4A: 0.51 ± 0.04, $p < 0.001$; DS2UA: 0.99 ± 0.03, $p = 0.89$; HA: 0.93 ± 0.04, $p = 0.18$; Figure 1C). Likewise, DS1-derived neurons co-cultured with DS astroglia (DS1A or DS4A) showed significantly decreased FP-evoked Ca^{2+} amplitudes relative to neurons cultured alone (normalized $\Delta F/F$; DS1A: 0.66 ± 0.07, $p < 0.01$; DS4A: 0.43 ± 0.05, $p < 0.001$; DS2UA: 0.92 ± 0.04,

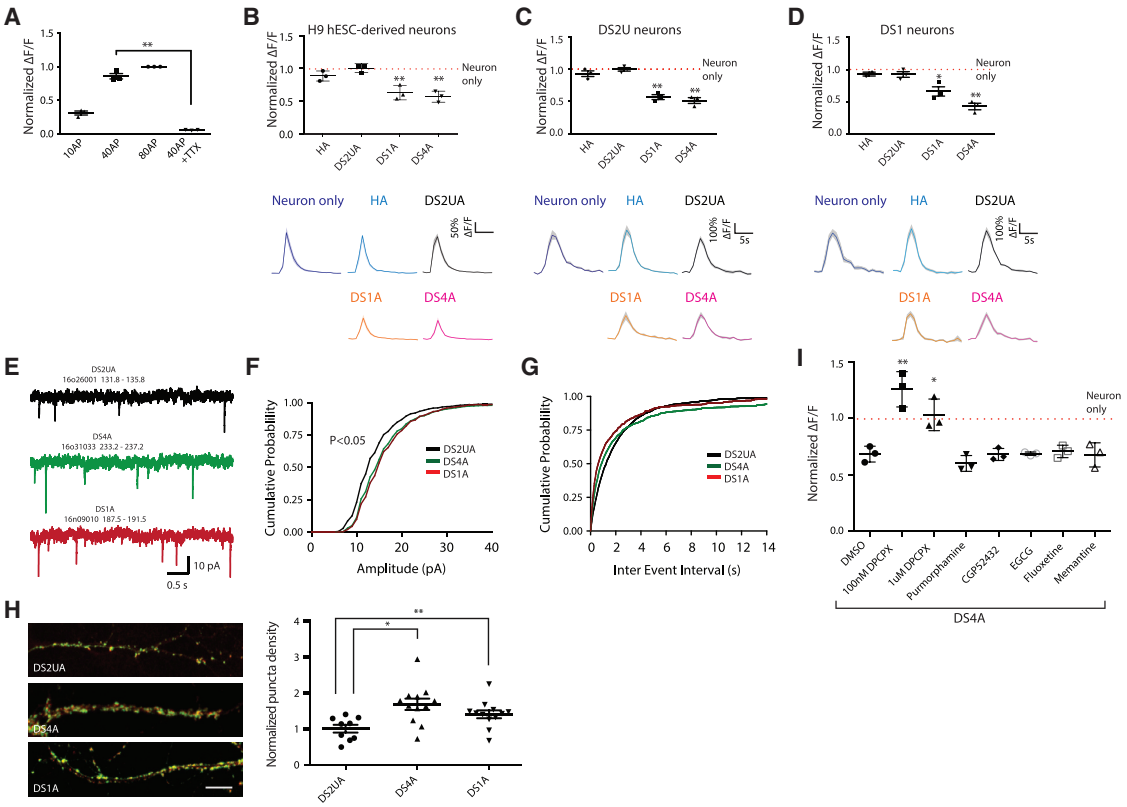

Figure 1. DS Astroglia Inhibit Neuronal Excitability during Co-culture

(A) The fluorescence changes (ΔF/F) of H9 hESC-derived neurons in response to a variety of FP stimuli; ΔF/F at 10 FPs, 40 FPs, and 40 FPs in the presence of 1 μM TTX were normalized to ΔF/F at 80 FPs.

(B–D) The responses of H9 hESC- (B), isogenic DS2U- (C), and DS1-iPSC- (D) derived neurons to FP stimuli (40 FPs at 30 Hz) when co-cultured with or without astroglia. ΔF/F induced by FP stimuli in the presence of astrocytes was normalized to that of neurons alone (red dotted lines). Representative traces showing Ca^{2+} transients triggered by FPs in neurons are shown (right panel).

(E) Example recordings of mEPSCs from 1 neuron from each group.

(F) Cumulative probability of the mEPSC amplitude shifted rightward in both DS4A and DS1A groups compared with the DS2UA group.

(G) No change was seen in the cumulative probability of the mEPSC inter-event interval.

(H) Representative images and quantification of puncta density expressing both synapsin and PSD95 (n = 3 images of immunostaining).

(I) The fluorescence changes of H9 hESC-derived neurons in response to 40 FPs stimuli when co-cultured with DS4A in the presence of DMSO or a series of drugs are shown and normalized to changes when co-cultured with DS2UA. For each cell line, n = 3 Ca^{2+}-imaging sessions (each session contains 3 fields of view). Error bars are shown as mean ± SEM, *p < 0.05, **p < 0.01.

p = 0.15; HA: 0.95 ± 0.03; p = 0.18; Figure 1D). Decreased neuronal activity in the presence of DS astroglia was observed under a variety of stimulation conditions but was most prominent during modest stimulation, such as 10FPs (Figure S2F). In addition, all co-cultured astrocytes significantly accelerated decay to baseline of evoked neuronal Ca^{2+} transients ($T_{0.5}$ = 1.62 ± 0.14 for neuron-alone; 1.25 ± 0.12, 1.11 ± 0.13, and 1.18 ± 0.1 for neurons co-cultured with DS2UA, DS1A, and DS4A, respectively; p < 0.01; Figure S2G). Taken together, DS astroglia inhibited neuronal excitability of neurons derived from either trisomy or disomy iPSC lines.

DS Astroglia Promote Synaptic Connectivity

As DS astroglia suppress neuronal activity, we next sought to determine whether DS astroglia influence synaptic function. DS astroglia were co-cultured with dissociated rat hippocampal neurons, and miniature excitatory postsynaptic currents (mEPSCs) were recorded in the presence of TTX, NMDA receptor antagonist D-AP5, and $GABA_A$ antagonist bicuculline (Figures 1E–1G, S2H, and S2I). Cumulative distribution plots showed that the mean amplitude of mEPSCs was significantly larger in neurons co-cultured with either DS4A or DS1A groups compared with control DS2UA (DS2UA: 14.21 ± 0.42; DS1A: 16.35 ± 0.78, p < 0.05; DS4A: 16.26 ± 0.73, p < 0.05; Figures 1F and S2H). mEPSC frequency was similar in all three groups, with a trend toward higher mEPSC frequencies in the neurons co-cultured with DS4A and DS1A groups (p = 0.204; DS2UA: 0.56 ± 0.06; DS1A: 1.29 ± 0.45; DS4A: 1.10 ± 0.36; Figures 1G and S2I). Next, using quantitative image analysis (Thomazeau et al., 2014), we found that synapse density significantly increased by 1.5- and 1.3-fold in neurons co-cultured with DS astrocytes (DS1A, p < 0.01 and DS4A, p < 0.05, respectively)

compared with those co-cultured with isogenic control astrocytes (Figure 1H). Taken together, these results suggest that DS astroglia are capable of modulating neuronal excitability as well as synaptic activity and density.

Pharmacological Rescue of Suppressed Neuronal Excitability

We next examined whether pharmacological drugs that block astrocyte-neuron communication could rescue the suppressed neuronal excitability. We first examined a panel of small-molecule drugs that have been shown to rescue synaptic abnormalities in DS mouse models (Busciglio et al., 2013). These compounds, including purmorphamine (sonic hedgehog agonist), CGP52432 ($GABA_BR$ antagonist), epigallocatechin-3-gallate (EGCG) (DYRK1A inhibitor), fluoxetine (serotonin reuptake inhibitor), and memantine (NMDA receptor antagonist), however, failed to rescue decreased neuronal activity associated with DS astroglia (normalized $\Delta F/F = 0.60 \pm 0.04$, 0.68 ± 0.03, 0.70 ± 0.02, 0.71 ± 0.03, and 0.68 ± 0.06 from purmorphamine to memantine; $p = 0.22$, 0.95, 0.73, 0.67, and 0.93; $n = 3$; Figure 1I).

We next tested whether suppressed neuronal excitability is caused by adenosine-mediated signaling that has been shown to inhibit synaptic activity (Adair, 2005; Delekate et al., 2014; Kawamura and Kawamura, 2011; Koizumi, 2010; Nam et al., 2012). We treated H9 neurons co-cultured with DS astroglia (DS4A) with a G_i-coupled A_1 adenosine receptor antagonist, followed by imaging FP-evoked neuronal activity. In particular, the A_1 receptor antagonist DPCPX fully rescued suppressed neuronal activity, especially at lower concentrations (100 nM: normalized $\Delta F/F = 1.20 \pm 0.09$, $p < 0.01$; 1 μM: 0.98 ± 0.08, $p < 0.05$; $n = 3$; Figure 1I). We also treated H9 hESC derived with 100 μM adenosine, which resulted in suppressed neuronal activity after one hour incubation (normalized $\Delta F/F$ of 100 μM adenosine to without adenosine = 0.20 ± 0.06; $p < 0.01$; Figure S2J). Furthermore, astroglia-conditioned medium (ACM) from DS4A also showed a trend of suppressed neuronal excitability compared to no ACM (Figure S2K).

DS Astroglia Exhibit Abnormally Frequent Spontaneous Ca^{2+} Fluctuations

Astrocytic Ca^{2+} signaling has been proposed to modulate neural-circuit activity and structure (Anderson et al., 2016; Bazargani and Attwell, 2016); the suppressed excitability of neurons was specific to DS astroglia and could be rescued when astrocyte-neuron communication was blocked by an adenosine receptor antagonist. This evidence led us to further investigate Ca^{2+} dynamics in astroglia. We focused on optical recordings of calcium dynamics in astroglia using GCaMP6m (Chen et al., 2013). We used the machine-learning software Functional Astrocyte Phenotyping (FASP) (Wang et al., 2016) to facilitate automated detection and analysis of complex Ca^{2+} dynamics in astroglia.

The differentiated astroglia indeed displayed prominent spontaneous Ca^{2+} transients, which were frequently periodic and especially apparent in DS astroglia (Figure 2A; Videos S1 and S2). DS astroglia exhibited significantly more (7- to 34-fold) Ca^{2+} transients than control isogenic astroglia (averaged number of calcium transients in a 5-min imaging session: DS1A: 58 ± 6, DS4A: 275 ± 34, DS2UA: 8 ± 2; mean ± SEM; $p < 0.0001$; unpaired t test; $n = 9$ imaging sessions; Figure 2B). The average amplitude ($\Delta F/F$; DS1A: 1.45 ± 0.2, DS4A: 0.98 ± 0.15; $p < 0.01$; Figure 2C) and frequency (transients/min; DS1A: 0.41 ± 0.10, DS4A: 0.88 ± 0.16; $p < 0.01$; Figure 2D) of Ca^{2+} transients were significantly different between DS1A and DS4A, whereas the kinetics were similar ($T_{1/2}$, s; DS1A: 8.59 ± 1.01; DS4A: 6.98 ± 0.90; $p = 0.18$; Figure 2E). These disparities are potentially due to epigenetic changes between the cell lines.

Inositol triphosphate (IP_3)-triggered Ca^{2+} release from the endoplasmic reticulum (ER) is considered a primary mechanism responsible for intracellular global Ca^{2+} waves (Tong et al., 2013). Application of the IP_3 receptor (IP_3R) antagonist 2-aminoethoxydiphenyl borate (2-APB) abolished spontaneous Ca^{2+} fluctuations (Figures 2F–2I), as did depletion of intracellular stores by cyclopiazonic acid (CPA), suggesting that IP_3-ER Ca^{2+} underlies both spontaneous and evoked events in DS astroglia.

Wavefront analysis of the spontaneous events revealed 33 clusters of cells (Figure S3A, left) with temporally correlated Ca^{2+} fluctuations (Figure S3A, right) that were spatially intermingled (Figure S3B), suggesting that Ca^{2+} fluctuations do not propagate to adjacent cells. To further examine whether spontaneous fluctuations travel between cells, we performed Ca^{2+} imaging in a mixed culture of GCaMP6m-expressing control isogenic astroglia with unlabeled DS4A in a variety of ratios. Culturing with DS astroglia did not significantly increase the number of Ca^{2+} transients in control isogenic astroglia, even with a 10-fold excess of DS4A (Figure S3C), suggesting that spontaneous Ca^{2+} fluctuations were not induced in previously silent control isogenic cells. In addition, application of 10 μM *n*-octanol, a gap junction blocker, showed no effect on Ca^{2+} fluctuations (Figure S3D).

Acutely purified human astrocytes acquire sensitivity to extracellular cues, such as neurotransmitter ATP and glutamate (Zhang et al., 2016). To exclude the possibility that differences in functional maturation of differentiated astroglia contribute to suppressed neuronal excitability, we examined transmitter-evoked Ca^{2+} responses of DS astroglia and compared with isogenic controls. Only previously, silent astrocytes were selected for quantification of evoked responses in order to differentiate evoked from spontaneous activity. Both DS and control isogenic astroglia responded robustly to ATP (representative traces of evoked Ca^{2+} transients shown in Figures S3E and S3F) in terms of the number and amplitude of evoked intracellular Ca^{2+} transients. Similarly, both DS astroglia and control isogenic astroglia responded to glutamate at micromolar concentrations (Figures S3G and S3H). Thus, DS and control astroglia respond similarly to neurotransmitters, further suggesting that Ts21 does not influence functional maturation of differentiated astrocytes.

Blocking Spontaneous Ca^{2+} Fluctuations in DS Astroglia Rescues Suppressed Neuronal Excitability

We tested whether the suppression of neuronal activity might be caused by the abnormally frequent spontaneous Ca^{2+} fluctuations observed in DS astroglia. Because pharmacological block of IP_3 receptors abrogated spontaneous Ca^{2+} waves (Figures 2F–2I), we knocked down (KD) the expression of *IP_3R2* in DS astroglia DS4A alone, the main *IP_3R* isoform in astrocytes, with

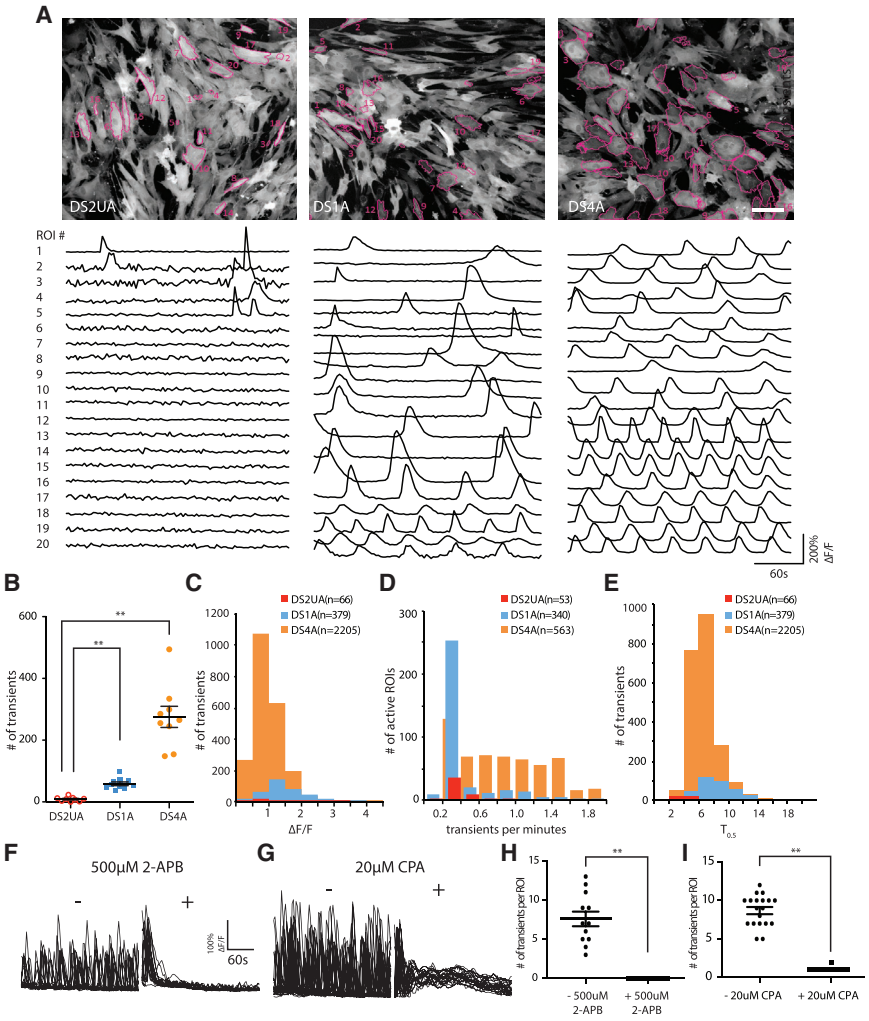

Figure 2. Imaging Ca^{2+} Events in Human-iPSC-Derived Isogenic and DS Astroglia

(A) Spontaneous Ca^{2+} responses in isogenic DS2UA and two DS astroglia (DS1A and DS4A). Representative ROIs (n = 20) in the field of view showing Ca^{2+} fluctuations in DS2UA, DS1A, and DS4A. All ROIs were detected using FASP and marked with magenta outlines. The scale bar represents 100 μm.

(B) DS1A and DS4A displayed a significantly increased number of Ca^{2+} fluctuations in 5 min of imaging sessions compared with DS2UA (9 independent imaging sessions).

(C–E) Features of Ca^{2+} fluctuations in DS astroglia: averaged kinetics (C), frequency (D), and propagation speed (E) of DS astroglia. Data were collected from 81 cells of DS1A and 188 cells of DS4A.

(F–I) The Ca^{2+} fluctuations in DS4A could be abolished by incubation with IP_3R antagonist (500 μM 2-APB; 17 ROIs; F and H) or depleting ER Ca^{2+} store (20 μM CPA; 23 ROIs; G and I).

Error bars are shown as mean ± SEM, *$p < 0.05$, **$p < 0.01$.

short hairpin RNAs (shRNAs). *IP_3R2* KD in DS astroglia DS4A (Figure 3B) significantly reduced the number of active regions of interest (ROIs) showing spontaneous Ca^{2+} transients (scrambled shRNA: 61.0 ± 3.8; *IP_3R2* shRNA-1: 21.3 ± 2.4 [35%]; *IP_3R2* shRNA-2: 14.3 ± 1.8 [24%]; $p < 0.001$; Figures 3A and 3C).

We then imaged the activity of neurons co-cultured with DS4A astroglia with *IP_3R2* knocked down, which rescued the reduced amplitude of evoked neuronal Ca^{2+} transients (measured as normalized ΔF/F; *IP_3R2* shRNA-1: 0.91 ± 0.0.4; shRNA-2: 0.93 ± 0.03) to the level of isogenic control astroglia (1.01 ± 0.04; $p = 0.28$). In contrast, DS4A with no shRNA (0.60 ± 0.05; $p < 0.01$) or control-scrambled shRNA (0.62 ± 0.04; $p < 0.01$) showed significantly decreased neural activity (Figure 3D). Therefore, elevated intracellular Ca^{2+} fluctuation mediated by IP_3R2 is necessary to suppress neuronal excitability.

Spontaneous Ca^{2+} Fluctuations in DS Astroglia Are Not Driven by Extracellular Cues

As elevated spontaneous astroglia Ca^{2+} activity directly contributed to suppressed neuronal activity, we next sought to determine the factors driving elevated Ca^{2+} activity in DS astroglia. We first performed single-cell analysis of gene expression related to Ca^{2+} signaling pathways (Figure S4A) in DS astroglia. We also monitored the expression of a panel of astrocytic markers to account for the differentiation state of individual cells (Figures S4A and S4B). We then performed unsupervised clustering analysis of the cells by their gene expression patterns. We found that DS astroglia (DS4A) clustered into two groups (Figure S4C), distinguished by elevated expression of Ca^{2+} handling genes, such as *ATP2B1*, *NCX1*, *RYR1/3*, *STIM1*, *NCLX*, *IP3R3*, *ORAI1*, and chromosome 21 gene *S100B* (Table S1). This suggests that a subset of DS astroglia may display elevated spontaneous Ca^{2+} fluctuations. In DS astroglia, astrocytic markers, such as *CD44*, *CX43*, *AQP4*, *NF1A*, and *ALDOC*, were not differentially expressed between the two clusters. In contrast, we failed to identify significant clustering (Figure S4D) of genes related to the Ca^{2+}-handling toolkit in control isogenic astroglia (DS2UA).

Moreover, from the single-cell gene analysis, we found that metabotropic glutamate receptors (*GRM1/2/3/4/5/6/7/8*) and purinergic receptors were elevated in a subset of DS4UA. We next investigated whether spontaneous fluctuations in DS astroglia could be modulated by pharmacological manipulation of these receptors. ATP treatment led to a 2-fold increase in the frequency and a 1.4-fold increase in the amplitude of spontaneous Ca^{2+} fluctuations in ~40% of ROIs (Figure 4A). However, treatment with P2-isotype-specific ATP receptor antagonists (PPADS for P2X; MRS2179 for P2Y; Figures 4B and S5A), non-specific P2 antagonists (suramin; Figure 4C), or an adenosine A_1-receptor antagonist (DPCPX; Figure 4D) had no significant effect on spontaneous Ca^{2+} fluctuations, suggesting that, although ATP can

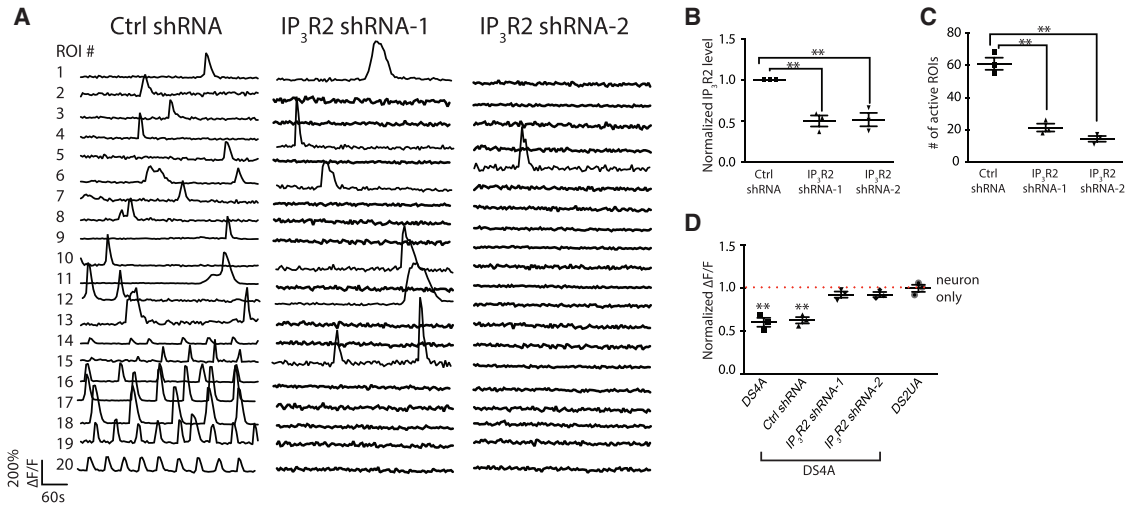

Figure 3. DS Astroglial Ca^{2+} Fluctuations Are Regulated by IP_3R-ER Pathway

(A–C) The Ca^{2+} events in DS4A were significantly decreased by knocking down the expression of *IP_3R*. Representative ROIs (n = 20) showing Ca^{2+} fluctuations in DS4A expressing scrambled shRNA (ctrl shRNA) and two shRNAs for *IP_3R* (IP_3R shRNA-1/2; A). Real-time PCR confirmed the decreased expression of *IP_3R* in the presence of *IP_3R* shRNAs (3 RNA samples; B), corresponding to a decreased number of Ca^{2+} events in 5 min (3 imaging sessions; C).

(D) Normalized fluorescence changes of H9 hESC-derived neurons in response to 40 FPs co-cultured with DS4A or DS4A expressing scrambled or *IP_3R* shRNAs to those of neurons alone (dotted red line).

Error bars are shown as mean ± SEM, *p < 0.05, **p < 0.01.

modulate spontaneous Ca^{2+} events in DS astroglia, it is not necessary to evoke them. CHPG (a selective mGluR5 agonist) showed no significant effects on amplitude, frequency, or kinetics of spontaneous Ca^{2+} fluctuations (Figure S5B). Similarly, mGluR5-selective (MPEP), non-selective mGluR (MCPG), and mGluR2/3-selective (LY341495) antagonists, as well as a glutamate transporter inhibitor (TFB-TBOA), also had no effect (Figures 4E and S5C–S5E). The TRPA1 channel antagonist HC030031 also had no significant effect on spontaneous Ca^{2+} fluctuations (Figure 4F), consistent with the lack of microdomain Ca^{2+} activity observed (Shigetomi et al., 2011). In summary, whereas both intrinsically and extrinsically driven calcium transients depend on IP_3-mediated release from ER stores, our results suggest that spontaneous fluctuations are unlikely to be driven, though can be modified, by extracellular cues.

S100B Regulates Spontaneous Ca^{2+} Fluctuations in DS Astroglia

From gene analysis, we also noticed that *S100B*, a Ca^{2+}-binding protein located on HSA21 and primarily expressed in astrocytes, was one of the top genes differentially expressed across DS4A cells. S100B elicits neurotrophic effects and regulates synaptic plasticity and rhythmic neuronal activity by chelating extracellular calcium (Morquette et al., 2015; Nishiyama et al., 2002). Given the particular interest in the context of Ts21 DS, we thus asked whether elevated S100B might contribute to the spontaneous intracellular Ca^{2+} fluctuations in DS astroglia.

We first quantified the expression level of *S100B* in Ts21-derived astroglia. qRT-PCR analysis showed an averaged 11-fold greater expression of *S100B* in DS astroglia (DS1A and DS4A) compared with control isogenic DS2UA cells (Figure S1C). Expression of S100B protein was enriched in DS astroglia compared to DS2UA (Figures 5A and 5B; 9.9- and 10.7-fold increased expression S100B for DS1A and DS4A, respectively, compared to DS2UA).

We next selectively knocked down *S100B* in DS4A and performed Ca^{2+} imaging. Using mCherry as a proxy for the extent of *S100B* KD, we used fluorescence-activated cell sorting (FACS) to select the top 15% of cells showing potent *S100B* KD and use the bottom 15% of cells as a control group showing normal S100B levels (Figures 5C–5F). The *S100B* KD population showed a 3.5-fold decrease in spontaneous Ca^{2+} transients during a 5-min window ($p < 0.001$; Figures 5D and 5F), which corresponds to ~10-fold lower S100B levels compared to the control group ($p < 0.001$; Figure 5E). These data suggest that S100B modulates spontaneous Ca^{2+} fluctuations in DS astroglia.

Given the reported role of secreted S100B protein in modulating neural activity, we incubated the cultures with antibodies against S100B or Tuj1 (without permeabilization). After 10 min incubation, there was no effect on spontaneous Ca^{2+} events of either antibody (Figure 5G), suggesting that the spontaneous Ca^{2+} events are mediated by intracellular S100B.

We then asked whether overexpression of S100B protein would also modulate spontaneous Ca^{2+} fluctuations. We observed 2-fold increase in the number of Ca^{2+} transients when S100B was overexpressed in DS1A (Figures 5H and 5I; $p < 0.01$), in which the number of spontaneous Ca^{2+} transients is less abundant than DS4A.

Finally, we examined whether DS astroglia with spontaneous Ca^{2+} fluctuations alleviated by *S100B* KD still suppressed neuronal excitability. We recorded evoked Ca^{2+} events in response to FP stimuli in H9 neurons co-cultured with DS4A with or without *S100B* KD. H9 neurons co-cultured with DS4A with potent *S100B* KD displayed significantly larger (1.7-fold;

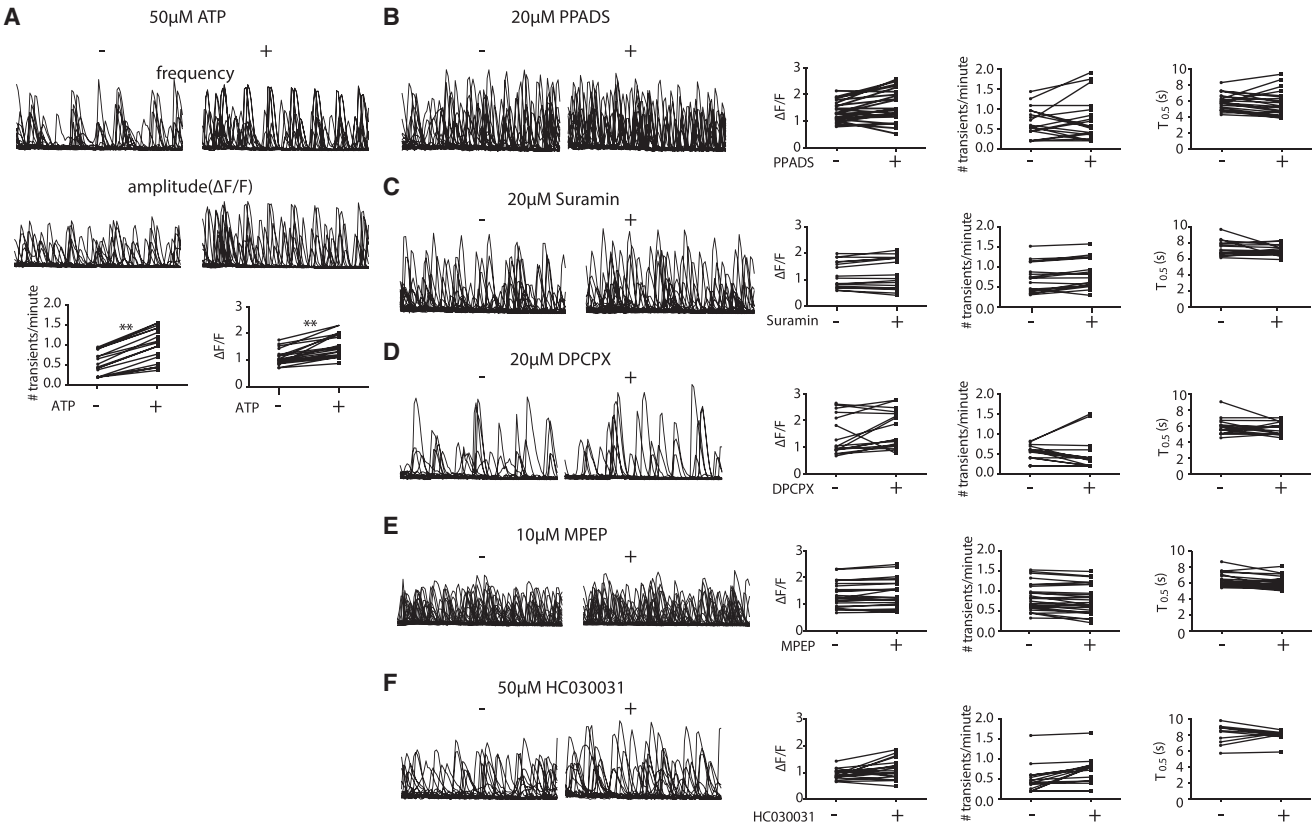

Figure 4. Spontaneous Fluctuations in DS Astroglia Could Not Be Modulated by Pharmacological Manipulation

(A) ATP increased the frequency and amplitude of Ca^{2+} events in previously active cells (20 ROIs; $p < 0.01$).

(B and C) Purinergic receptor antagonist (20 μM PPADS; 25 ROIs, B; and 20 μM suramin; 18 ROIs, C) failed to modulate the Ca^{2+} fluctuations in DS4A.

(D–F) A1 adenosine receptor antagonist (DPCPX 20 μM; 18 ROIs; D), mGluR5 antagonist (10 μM MPEP; 42 ROIs; E), and TRPA inhibitor (50 μM HC030031; 20 ROIs; F) failed to modulate the Ca^{2+} fluctuations in DS4A. (Left) Representative traces are shown. (Right) Quantification of amplitude, frequency, and kinetics is shown.

*$p < 0.01$, **$p < 0.01$.

$p < 0.01$) neural activity than those without *S100B* KD (Figure 5J), suggesting that *S100B* KD successfully rescued neuronal activity suppressed by DS4A. Thus, we conclude that blocking Ca^{2+} fluctuations in DS astroglia by genetic ablation of either *IP_3R2* or *S100B* is sufficient to rescue the excitability decreases of co-cultured neurons.

DISCUSSION

Combining human stem cell technology with Ca^{2+} imaging and quantitative analysis tools provides a powerful platform to study neuron-astrocyte interaction in both physiological and pathological conditions, especially at early developmental stages. Using this platform, we imaged and characterized the effect of Ts21-iPSC-derived astroglia on neuronal networks. DS astroglia produced structural and functional deficits in co-cultured neurons. Specifically, neurons co-cultured with DS astroglia displayed decreased global excitability. Such decreased global excitability of neurons corresponded with increased amplitudes of post-synaptic activity and synaptic density, consistent with accepted mechanisms of homeostatic synaptic plasticity and synaptic scaling (Turrigiano, 2012). Our data are in line with a rodent DS model study, in which the dendritic spine density and mEPSC amplitude increased although frequency of mEPSCs remained unchanged in prefrontal cortical pyramidal neurons (Thomazeau et al., 2014). Though abnormal synaptic morphology, such as reduced synaptic density, has been reported in other iPSC-derived DS models and in Ts65Dn adult mice, none of these studies have examined the function of astrocytes and potential effect imposed by astrocytes at early stages of brain development. Therefore, the effect of DS astrocytes on synaptic properties is worth further investigating across the whole spectrum of neuronal differentiation and development in iPSC-based DS models. In addition, transplantation of DS astrocytes into rodent models can be performed to directly examine the effect imposed by astrocytes on synaptic properties at early stages of brain development.

We further showed functional differences between DS astroglia and control isogenic astroglia in terms of intracellular Ca^{2+} dynamics. We observed elevated spontaneous Ca^{2+} fluctuations that are frequent and periodic only in DS-derived astroglia, but not in an isogenic control cell. These aberrant Ca^{2+} fluctuations in DS astroglia are necessary to drive suppression of global

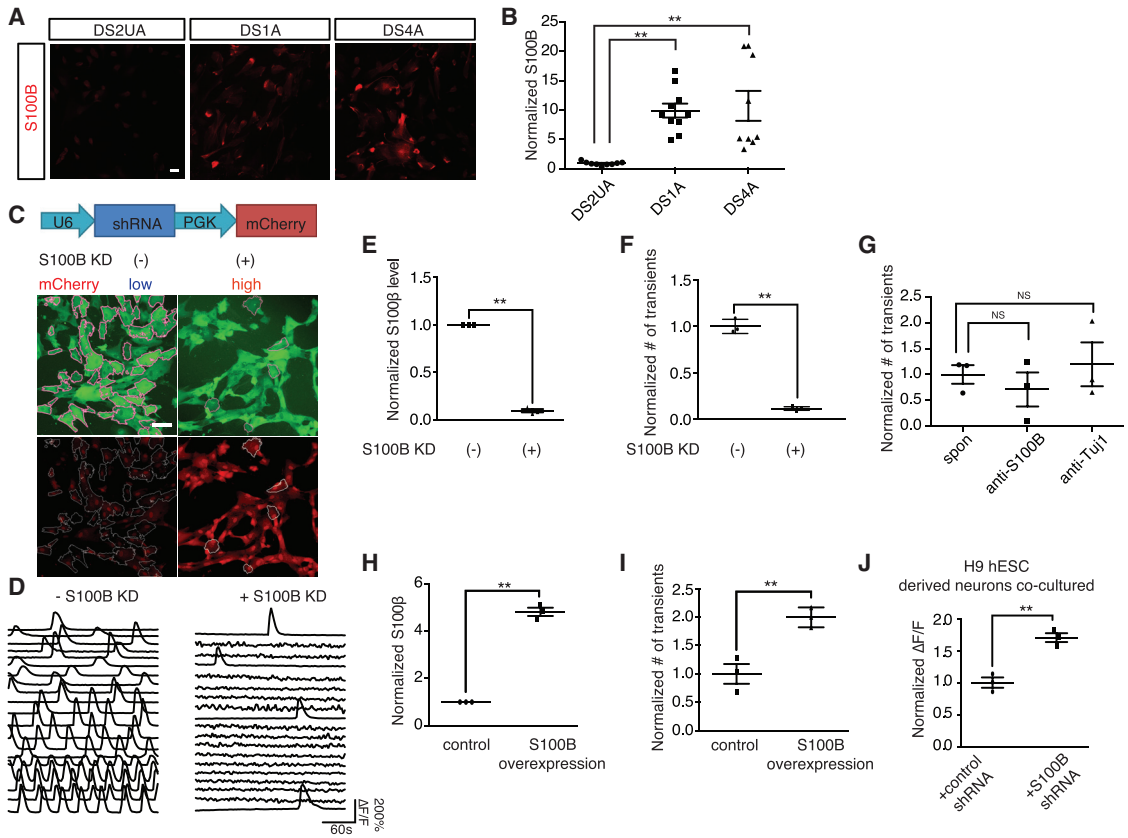

Figure 5. S100B Regulates Spontaneous Ca^{2+} Fluctuations in DS Astroglia

(A and B) Immunostaining of S100B in iPSC-derived astroglia (A) revealed increased expression in DS astroglia normalized to isogenic DS2UA (three images of immunostaining; 12.5% ± 1.0% for DS2UA; 80.4% ± 1.8% for DS1A; 75.3% ± 2.9% for DS4A; $p < 0.01$; B). Scale bar: 10 μm.

(C) Schematic representation of lentiviral construct encoding *S100B* shRNA-nls-mCherry. Scale bar: 50 μm.

(D) Representative ROIs (n = 20) highlighted in (C) showing spontaneous Ca^{2+} fluctuations in populations of DS4A without (left) and with *S100B* KD (right). The scale bars represent 50 μm.

(E and F) The *S100B* expression levels normalized to without *S100B* KD (3 RNA samples; E) and the number of Ca^{2+} events (3 imaging sessions of 5 min; F) with and without *S100B* KD are shown.

(G) Extracellular application of anti-S100B antibody did not influence the number of spontaneous Ca^{2+} fluctuations in DS4A (3 imaging sessions).

(H and I) Overexpression of S100B increased the number of Ca^{2+} events in DS1A. qPCR analysis confirmed elevated expression of S100B in DS1A when S100B was overexpressed (3 RNA samples; 4.8- ± 0.2-fold normalized to empty vector group; $p < 0.01$; H). 2-fold more Ca^{2+} events in 5 min were detected in DS1A when S100B was overexpressed normalized to control (3 imaging sessions; I).

(J) Blocking intracellular Ca^{2+} events by *S100B* KD increased activity of H9 hESC-derived neurons co-cultured with DS4A. The fluorescence changes of H9 hESC-derived neurons in response to 40 FPs stimuli co-cultured with DS4A with *S100B* shRNA normalized to DS4A with control shRNA are shown. Error bars are shown as mean ± σEM, *$p < 0.05$, **$p < 0.01$.

excitability in co-cultured neurons, as evidenced by rescue by genetic or pharmacological block.

What causes aberrant Ca^{2+} fluctuations in DS astroglia? Here, we demonstrate that overexpression of cellular S100B in DS astroglia mediates elevated spontaneous Ca^{2+} fluctuations (Figures 5H and 5I), which subsequently regulate neuronal excitability (Figure 5J). This finding is of particular interest, as S100B is a Ca^{2+}-binding protein. Previous research (Barger et al., 1992) has shown that secreted S100B stimulates a rise in intracellular Ca^{2+} concentration in both neurons and glia. Furthermore, extracellular S100B regulates the firing patterns of neurons by reducing extracellular Ca^{2+} concentrations (Morquette et al., 2015). In our studies, extracellular S100B did not influence spontaneous Ca^{2+} fluctuations in DS astroglia, whereas cytosolic of S100B did. Further investigation is necessary to parse the various functions of secreted and cytosolic S100B in healthy and disease model astrocytes and neurons.

A major open question in DS research is the mechanism by which the overdose of hundreds of genes on HSA21 disrupts brain function. To date, several candidate genes have been identified, including *DYRK1A*, *SIM2*, *DSCAM*, *KCNJ6*, *NKCC1*, and *miR-155* (Deidda et al., 2015; Dierssen, 2012; Wang et al., 2013; Table S1). Overexpression of S100B, at the distal end of the HSA21 long arm, has been shown to generate reactive oxygen species (ROS) (Esposito et al., 2008) in human induced pluripotent stem cells (hiPSC)-derived DS astroglia, leading to neuronal apoptosis (Chen et al., 2014). Previous research reported that ROS induce lipid peroxidation, activate the PLC-IP_3R pathway, and cause

Ca^{2+} increases in astrocytes (Vaarmann et al., 2010). Indeed, we found that spontaneous Ca^{2+} activity was mediated by IP_3R2-regulated ER stores. Though we do not have direct evidence to link S100B, ROS, and PLC-IP_3R, S100B might mediate perturbed Ca^{2+} dynamics via ROS in DS astroglia.

Our study provides additional evidence to support the hypothesis that astrocytic Ca^{2+} signaling modulates neural activity, critical for brain function during development. A grand challenge is to elucidate the pathways regulating astrocyte-neuron interplay during development. In the present study, our results indicate that astrocyte-neuron interaction via purinergic signaling might be a significant contributor linking aberrant astrocytic Ca^{2+} to neuronal functional deficits in DS. We showed that treatment with 100 μM adenosine in H9 hESC-derived neurons without the presence of astrocytes suppressed neuronal activity. Furthermore, treatment with DPCPX, an adenosine A_1 receptor antagonist, rescued the suppressed Ca^{2+} activity of H9 hESC-derived neurons co-cultured with DS astroglia (Figure 1I). Previous research has shown that adenosine predominantly inhibits synaptic activity via A_1 receptors (Delekate et al., 2014; Koizumi, 2010; Nam et al., 2012). However, future efforts should focus on further elucidating the source of release and other co-factors involved in the neuronal inhibition.

In conclusion, the combination of a human iPSC DS model with functional imaging and pharmacological and genetic manipulation provides a platform for quantitative measurement of human cellular physiology and for mechanistic studies of disease pathophysiology. Though animal models of neurological disorders play an important role in studying the effects of specific genetic and experimental perturbations and in testing potential treatments, they often fail to faithfully recapitulate the full spectrum of human phenotypes, which can lead to false conclusions owing to molecular and cellular differences between the systems. Future improvements to iPSC models will include 3-dimensional culture (Paşca et al., 2015), multi-color imaging, and incorporating genetically encoded indicators for other molecules and cellular states (e.g., glutamate; Marvin et al., 2013). Our imaging platform can be applied to the study of other neurological diseases as well, even to the level of testing specific drug combinations on neuron-astrocyte co-cultures developed from single healthy or diseased individuals.

EXPERIMENTAL PROCEDURES

Neural Differentiation of Human ESCs and iPSCs

H9 human ESCs were obtained from WiCell (Madison, WI). Control isogenic trisomy 21 and euploid iPSCs, DS1, DS2U, and DS4, were engineered in Dr. Anita Bhattacharyya's lab, as previously described (Weick et al., 2013). H9 ESCs and iPSCs were maintained on Matrigel (Becton Dickinson; 356234) in mTeSR1 medium (StemCell Technologies; 05850). Mycoplasma contamination was routinely tested. We used previously described protocols for neural differentiation (Zhang et al., 2001), with minor modifications. Briefly, following detachment of neuroepithelia from adherent conditions at day 14, neurospheres were expanded in fibroblast growth factor (FGF)/epidermal growth factor (EGF) (10 ng/mL). Large spheres were disaggregated into smaller clusters approximately every two weeks until day 90. 20–25 neurospheres or 2.5 × 10^4 cells/cm^2 were seeded on 35-mm Matrigel-coated glass-bottom dishes (MatTek; P35G-1.0-14-C), and once confluent, neurospheres were cultured in neuronal medium (neurobasal medium, 21103-049; 1% N-2 supplement, 17502-048, 2% B-27 supplement, 17504-044; 10 ng/mL BDNF [450-02]; and GDNF [450-10]) for 40 days. Medium components were purchased from Thermo Fisher Scientific and cytokines from Peprotech. Inhibitors of SMAD signaling (10 μM SB431542 and 100 nM LDN193189; Tocris Bioscience) were added for the first 6 days to promote neural induction (Chambers et al., 2009).

Derivation and Culture of Astrocytes

Control isogenic and DS iPSCs were differentiated into neural progenitors and cultured similar to neural differentiation with the following modifications. Astrospheres were then plated at a concentration of 500,000 cells/mL in 12 mL of media in T75 flasks and allowed to adhere to fibronectin-coated dishes (Sigma; F0895). After confluent, astrospheres were dissociated into single cells and cultured in an optimized commercial medium for human primary astrocytes (ScienCell Research Laboratories; 1801). HAs were from ScienCell Research Laboratories (1800). We performed karyotype analysis on DS1-, DS4-, and DS2U-derived astroglia, prior to and after the Ca^{2+} experiments (Cell Line Genetics). The cell size was analyzed by randomly selecting 5 cells from 3 bright field images (ImageJ).

Ca^{2+} Imaging and Analysis in Astrocytes

Primary astrocytes or iPSC-derived astrocytes were seeded onto 8-well slides (Ibidi; 80826), coated with fibronectin, and infected with lentiviruses encoding *EF1α*-GCaMP6m and then subjected to Ca^{2+} imaging. For *IP_3R2* KD, DS4A cells were infected with lentiviruses encoding shRNA and GCaMP6m; Ca^{2+} imaging followed. For *S100B* KD, DS4A cells were infected with lentiviruses encoding shRNA, sorted into 2 populations by FACS according to mCherry intensity, and infected with GCaMP6m for each population; Ca^{2+} imaging followed. For each cell line, 3 Ca^{2+}-imaging sessions (each session contains 3 fields of view) were collected from independent samples. For mixed cultures of control isogenic and DS astrocytes, control isogenic DS2UA were first infected with lentiviruses expressing *EF1α*-GCaMP6m and then seeded with DS4A, followed by Ca^{2+} imaging. Three days post-infection, frame scans were acquired at 2 Hz (512 × 512 pixels) for a period of 300 s. All imaging was done using a Zeiss LSM 710 confocal microscope (20× magnification; numerical aperture [N.A.] = 0.8 objective). Agonists or antagonists (Tocris) were added at frame 10 during continuous imaging. For quantification of ATP and glutamate-evoked activity, to eliminate the confound of spontaneous activity, only ROIs that were silent during the initial imaging period were analyzed for a response to added ATP or glutamate. Furthermore, we ensured that these evoked responses were time locked to agonist application.

Because of these complex spatiotemporal patterns of Ca^{2+} dynamics in astrocytes, we developed a computational tool (FASP; Wang et al., 2016) to quantitatively and automatically analyze the large-scale imaging datasets to ensure that the analysis is identical and objective for all cells and across experiments. Additional details are in the Supplemental Information.

Neuron-Astrocyte Co-culture and Astrocyte-Conditioned Media Incubation

Differentiated neurons were infected with lentiviruses expressing *Synapsin-1*-GCaMP6m. Two days post-infection, astrocytes were seeded on top of neurons to establish co-culture. Neurons were seeded with astrocytes at 1:1 at 5 × 10^4 in 35 mm on glass bottom dishes in 2 mL of medium or with 100 μg/mL of astrocyte-conditioned media in 8-well μ-slide dishes in 250 μL of media. After 3–7 days, infected neurons were stimulated using a custom-built field stimulator with platinum wires or 50 μM glutamate. Field stimuli were delivered as 40 V, 30 Hz, 1 ms pulses for the following trains: 10, 20, 40, and 80 field stimuli in Hank's balanced salt solution (HBSS) with 2 mmol $CaCl_2$ and $MgCl_2$. When chemicals were used, they were applied 3 days prior to imaging, except DPCPX and adenosine, which was acutely applied 1 hr prior to imaging. All chemicals were purchased from Tocris or Sigma.

Single-Cell Expression

DS astrocytes were digested and sorted by FACS to get rid of cell debris and dead cells. The cell suspension was loaded onto a C1 Single-Cell Auto Prep Array for mRNA Seq (10–17 μm; Fluidigm; 100-5760), and single cells were captured and lysed to get cDNA on Fluidigm's C1 platform. Gene expression patterns of single cells (n = 46) were studied using the 48.48 Dynamic Array Chip for Gene Expression following the manufacturer's instructions (Fluidigm; BMK-M48.48).

Animals

Animal studies were conducted in compliance with the Guide for the Care and Use of Laboratory Animals of the National Institutes of Health and approved by the Institutional Animal Care and Use Committee (IACUC) at the University of California, Davis or the relevant institutional regulatory body.

Statistical Analysis

All values are shown as mean ± SEM. To determine significant differences between groups, comparisons were made using a two-tailed unpaired t test. For mEPSC analysis, a one-way ANOVA was used to compare mEPSC amplitude and frequency among groups, followed by Fisher's least significant difference (LSD) pairwise comparison when appropriate. For single-cell expression analysis, a permutation test was applied for unsupervised clustering, and the differences of each gene between the two clusters were determined using two-sample unpaired Wilcoxon rank-sum test. A p value smaller than 0.05 was accepted for statistical significance $p < 0.01$ (**) or 0.05 (*). The sample size for each experiment was determined either by power analysis (2-sample, 2-sided equality) or by referring to the sample size in similar studies (Chen et al., 2014; Zhang et al., 2016). For Ca^{2+}-imaging experiments, imaging sessions were collected from at least 3 batches of cells, and ROIs were selected either automatically by FASP for astrocyte Ca^{2+} imaging or manually for neuronal Ca^{2+} imaging. For gene expression, RNA samples from three batches of cells were used. For immunostaining analysis, three batches of cells were fixed and five fields of view from each sample were selected for imaging and analyzed blinded. No randomization was used. No data were excluded.

SUPPLEMENTAL INFORMATION

Supplemental Information includes Supplemental Experimental Procedures, five figures, one table, and two videos and can be found with this article online at https://doi.org/10.1016/j.celrep.2018.06.033.

ACKNOWLEDGMENTS

This work was supported by the Hartwell Foundation Individual Biomedical Award (L.T.), NIH DP2MH107056 (L.T.), NIH R21NS095325 (L.T.), NIH R01MH110504 (L.T. and G.Y.), NSF1750931 (G.Y.), NIH R03 HD064880 (A.B.), National Institute of General Medical Sciences (NIGMS) 1P20GM109089-01A1 (J.W.), National Institute of Neurological Disorders and Stroke (NINDS) R21NS093442-01 and NSF7566685 (J.W.), and National Institute on Deafness and Other Communication Disorders (INCD) R01HD09325 (W.D.). This project was supported by the University of California, Davis, Flow Cytometry Shared Resource Laboratory with technical assistance from Ms. Bridget McLaughlin and Mr. Jonathan Van Dyke. We would like to give special thanks to Dr. Bart Borghuis for generously sharing the FluoAnalyzer codes, Dr. Karen Zito for critical input, Dr. Brett Mensh for critical discussions, and Lisa Makhoul for editorial assistance.

AUTHOR CONTRIBUTIONS

L.T., G.O.M., and G.S. conceived, designed, and executed the study. A.B. generated DS and isogenic iPSC lines, and J.W. generated astrocytic progenitors. G.O.M. and G.S. differentiated neurons and astroglia, developed co-culture system, and performed calcium imaging and histological experiments. G.Y., YinxueWang, and Yizhi Wang analyzed astrocytic Ca^{2+}-imaging data, synapse immunostaining, and single-cell profiling. G.J.B. provided algorithms for neuronal Ca^{2+}-imaging analysis. J.S. and C.-Y.C. performed electrophysiological recording of neurons. S.P. contributed to the production of lentiviral vectors. E.K.U. contributed to figures. G.O.M., G.S., and L.T. wrote the manuscript with critical input from A.B., J.W., W.D., G.Y., and L.L.L.

DECLARATION OF INTERESTS

The authors declare no competing interest.

Received: November 29, 2017
Revised: May 4, 2018
Accepted: June 7, 2018
Published: July 10, 2018

REFERENCES

Adair, T.H. (2005). Growth regulation of the vascular system: an emerging role for adenosine. Am. J. Physiol. Regul. Integr. Comp. Physiol. *289*, R283–R296.

Anderson, M.A., Burda, J.E., Ren, Y., Ao, Y., O'Shea, T.M., Kawaguchi, R., Coppola, G., Khakh, B.S., Deming, T.J., and Sofroniew, M.V. (2016). Astrocyte scar formation aids central nervous system axon regeneration. Nature *532*, 195–200.

Angulo, M.C., Kozlov, A.S., Charpak, S., and Audinat, E. (2004). Glutamate released from glial cells synchronizes neuronal activity in the hippocampus. J. Neurosci. *24*, 6920–6927.

Ballestín, R., Blasco-Ibáñez, J.M., Crespo, C., Nacher, J., López-Hidalgo, R., Gilabert-Juan, J., Moltó, D., and Varea, E. (2014). Astrocytes of the murine model for Down syndrome Ts65Dn display reduced intracellular ionic zinc. Neurochem. Int. *75*, 48–53.

Bambrick, L.L., Yarowsky, P.J., and Krueger, B.K. (2003). Altered astrocyte calcium homeostasis and proliferation in theTs65Dn mouse, a model of Down syndrome. J. Neurosci. Res. *73*, 89–94.

Barger, S.W., Wolchok, S.R., and Van Eldik, L.J. (1992). Disulfide-linked S100 beta dimers and signal transduction. Biochim. Biophys. Acta *1160*, 105–112.

Bazargani, N., and Attwell, D. (2016). Astrocyte calcium signaling: the third wave. Nat. Neurosci. *19*, 182–189.

Busciglio, J., and Yankner, B.A. (1995). Apoptosis and increased generation of reactive oxygen species in Down's syndrome neurons in vitro. Nature *378*, 776–779.

Busciglio, J., Pelsman, A., Wong, C., Pigino, G., Yuan, M., Mori, H., and Yankner, B.A. (2002). Altered metabolism of the amyloid β precursor protein is associated with mitochondrial dysfunction in Down's syndrome. Neuron *33*, 677–688.

Busciglio, J., Capone, G., O'Bryan, J., and Gardiner, K.J. (2013). Down syndrome: genes, model systems, and progress towards pharmacotherapies and clinical trials for cognitive deficits. Cytogenet. Genome Res. *141*, 260–271.

Cao, X., Li, L.-P., Wang, Q., Wu, Q., Hu, H.-H., Zhang, M., Fang, Y.-Y., Zhang, J., Li, S.-J., Xiong, W.-C., et al. (2013). Astrocyte-derived ATP modulates depressive-like behaviors. Nat. Med. *19*, 773–777.

Chambers, S.M., Fasano, C.A., Papapetrou, E.P., Tomishima, M., Sadelain, M., and Studer, L. (2009). Highly efficient neural conversion of human ES and iPS cells by dual inhibition of SMAD signaling. Nat. Biotechnol. *27*, 275–280.

Chen, T.-W., Wardill, T.J., Sun, Y., Pulver, S.R., Renninger, S.L., Baohan, A., Schreiter, E.R., Kerr, R.A., Orger, M.B., Jayaraman, V., et al. (2013). Ultrasensitive fluorescent proteins for imaging neuronal activity. Nature *499*, 295–300.

Chen, C., Jiang, P., Xue, H., Peterson, S.E., Tran, H.T., McCann, A.E., Parast, M.M., Li, S., Pleasure, D.E., Laurent, L.C., et al. (2014). Role of astroglia in Down's syndrome revealed by patient-derived human-induced pluripotent stem cells. Nat. Commun. *5*, 4430.

Das, I., and Reeves, R.H. (2011). The use of mouse models to understand and improve cognitive deficits in Down syndrome. Dis. Model. Mech. *4*, 596–606.

Deidda, G., Parrini, M., Naskar, S., Bozarth, I.F., Contestabile, A., and Cancedda, L. (2015). Reversing excitatory GABAAR signaling restores synaptic plasticity and memory in a mouse model of Down syndrome. Nat. Med. *21*, 318–326.

Delekate, A., Füchtemeier, M., Schumacher, T., Ulbrich, C., Foddis, M., and Petzold, G.C. (2014). Metabotropic P2Y1 receptor signalling mediates astrocytic hyperactivity in vivo in an Alzheimer's disease mouse model. Nat. Commun. *5*, 5422.

Di Giorgio, F.P., Boulting, G.L., Bobrowicz, S., and Eggan, K.C. (2008). Human embryonic stem cell-derived motor neurons are sensitive to the toxic effect of glial cells carrying an ALS-causing mutation. Cell Stem Cell *3*, 637–648.

Dierssen, M. (2012). Down syndrome: the brain in trisomic mode. Nat. Rev. Neurosci. *13*, 844–858.

Esposito, G., Imitola, J., Lu, J., De Filippis, D., Scuderi, C., Ganesh, V.S., Folkerth, R., Hecht, J., Shin, S., Iuvone, T., et al. (2008). Genomic and functional profiling of human Down syndrome neural progenitors implicates S100B and aquaporin 4 in cell injury. Hum. Mol. Genet. *17*, 440–457.

Garcia, O., Torres, M., Helguera, P., Coskun, P., and Busciglio, J. (2010). A role for thrombospondin-1 deficits in astrocyte-mediated spine and synaptic pathology in Down's syndrome. PLoS ONE *5*, e14200.

Huo, H.-Q., Qu, Z.-Y., Yuan, F., Ma, L., Yao, L., Xu, M., Hu, Y., Ji, J., Bhattacharyya, A., Zhang, S.-C., and Liu, Y. (2018). Modeling Down syndrome with patient iPSCs reveals cellular and migration deficits of GABAergic neurons. Stem Cell Reports *10*, 1251–1266.

Kawamura, M., Jr., and Kawamura, M. (2011). Long-term facilitation of spontaneous calcium oscillations in astrocytes with endogenous adenosine in hippocampal slice cultures. Cell Calcium *49*, 249–258.

Khakh, B.S., and McCarthy, K.D. (2015). Astrocyte calcium signaling: from observations to functions and the challenges therein. Cold Spring Harb. Perspect. Biol. *7*, a020404.

Koizumi, S. (2010). Synchronization of Ca2+ oscillations: involvement of ATP release in astrocytes. FEBS J. *277*, 286–292.

Krencik, R., Weick, J.P., Liu, Y., Zhang, Z.-J., and Zhang, S.-C. (2011). Specification of transplantable astroglial subtypes from human pluripotent stem cells. Nat. Biotechnol. *29*, 528–534.

Lee, S., Yoon, B.-E., Berglund, K., Oh, S.-J., Park, H., Shin, H.-S., Augustine, G.J., and Lee, C.J. (2010). Channel-mediated tonic GABA release from glia. Science *330*, 790–796.

Marchetto, M.C.N., Muotri, A.R., Mu, Y., Smith, A.M., Cezar, G.G., and Gage, F.H. (2008). Non-cell-autonomous effect of human SOD1 G37R astrocytes on motor neurons derived from human embryonic stem cells. Cell Stem Cell *3*, 649–657.

Marvin, J.S., Borghuis, B.G., Tian, L., Cichon, J., Harnett, M.T., Akerboom, J., Gordus, A., Renninger, S.L., Chen, T.-W., Bargmann, C.I., et al. (2013). An optimized fluorescent probe for visualizing glutamate neurotransmission. Nat. Methods *10*, 162–170.

Molofsky, A.V., Krencik, R., Ullian, E.M., Tsai, H.H., Deneen, B., Richardson, W.D., Barres, B.A., and Rowitch, D.H. (2012). Astrocytes and disease: a neurodevelopmental perspective. Genes Dev. *26*, 891–907.

Morquette, P., Verdier, D., Kadala, A., Féthière, J., Philippe, A.G., Robitaille, R., and Kolta, A. (2015). An astrocyte-dependent mechanism for neuronal rhythmogenesis. Nat. Neurosci. *18*, 844–854.

Mothet, J.-P., Pollegioni, L., Ouanounou, G., Martineau, M., Fossier, P., and Baux, G. (2005). Glutamate receptor activation triggers a calcium-dependent and SNARE protein-dependent release of the gliotransmitter D-serine. Proc. Natl. Acad. Sci. USA *102*, 5606–5611.

Murray, A., Letourneau, A., Canzonetta, C., Stathaki, E., Gimelli, S., Sloan-Bena, F., Abrehart, R., Goh, P., Lim, S., Baldo, C., et al. (2015). Brief report: isogenic induced pluripotent stem cell lines from an adult with mosaic down syndrome model accelerated neuronal ageing and neurodegeneration. Stem Cells *33*, 2077–2084.

Nam, H.W., McIver, S.R., Hinton, D.J., Thakkar, M.M., Sari, Y., Parkinson, F.E., Haydon, P.G., and Choi, D.-S. (2012). Adenosine and glutamate signaling in neuron-glial interactions: implications in alcoholism and sleep disorders. Alcohol. Clin. Exp. Res. *36*, 1117–1125.

Newman, E.A. (2001). Propagation of intercellular calcium waves in retinal astrocytes and Müller cells. J. Neurosci. *21*, 2215–2223.

Nishiyama, H., Knopfel, T., Endo, S., and Itohara, S. (2002). Glial protein S100B modulates long-term neuronal synaptic plasticity. Proc. Natl. Acad. Sci. USA *99*, 4037–4042.

Ota, Y., Zanetti, A.T., and Hallock, R.M. (2013). The role of astrocytes in the regulation of synaptic plasticity and memory formation. Neural Plast. *2013*, 185463.

Paşca, A.M., Sloan, S.A., Clarke, L.E., Tian, Y., Makinson, C.D., Huber, N., Kim, C.H., Park, J.-Y., O'Rourke, N.A., Nguyen, K.D., et al. (2015). Functional cortical neurons and astrocytes from human pluripotent stem cells in 3D culture. Nat. Methods *12*, 671–678.

Shi, Y., Kirwan, P., Smith, J., MacLean, G., Orkin, S.H., and Livesey, F.J. (2012). A human stem cell model of early Alzheimer's disease pathology in Down syndrome. Sci. Transl. Med. *4*, 124ra29.

Shigetomi, E., Tong, X., Kwan, K.Y., Corey, D.P., and Khakh, B.S. (2011). TRPA1 channels regulate astrocyte resting calcium and inhibitory synapse efficacy through GAT-3. Nat. Neurosci. *15*, 70–80.

Sloan, S.A., and Barres, B.A. (2014). Looks can be deceiving: reconsidering the evidence for gliotransmission. Neuron *84*, 1112–1115.

Thomazeau, A., Lassalle, O., Iafrati, J., Souchet, B., Guedj, F., Janel, N., Chavis, P., Delabar, J., and Manzoni, O.J. (2014). Prefrontal deficits in a murine model overexpressing the down syndrome candidate gene dyrk1a. J. Neurosci. *34*, 1138–1147.

Tong, X., Shigetomi, E., Looger, L.L., and Khakh, B.S. (2013). Genetically encoded calcium indicators and astrocyte calcium microdomains. Neuroscientist *19*, 274–291.

Tong, X., Ao, Y., Faas, G.C., Nwaobi, S.E., Xu, J., Haustein, M.D., Anderson, M.A., Mody, I., Olsen, M.L., Sofroniew, M.V., and Khakh, B.S. (2014). Astrocyte Kir4.1 ion channel deficits contribute to neuronal dysfunction in Huntington's disease model mice. Nat. Neurosci. *17*, 694–703.

Torres, M.D., Garcia, O., Tang, C., and Busciglio, J. (2018). Dendritic spine pathology and thrombospondin-1 deficits in Down syndrome. Free Radic. Biol. Med. *114*, 10–14.

Turrigiano, G. (2012). Homeostatic synaptic plasticity: local and global mechanisms for stabilizing neuronal function. Cold Spring Harb. Perspect. Biol. *4*, a005736.

Vaarmann, A., Gandhi, S., and Abramov, A.Y. (2010). Dopamine induces Ca2+ signaling in astrocytes through reactive oxygen species generated by monoamine oxidase. J. Biol. Chem. *285*, 25018–25023.

Wang, X., Lou, N., Xu, Q., Tian, G.-F., Peng, W.G., Han, X., Kang, J., Takano, T., and Nedergaard, M. (2006). Astrocytic Ca2+ signaling evoked by sensory stimulation in vivo. Nat. Neurosci. *9*, 816–823.

Wang, X., Zhao, Y., Zhang, X., Badie, H., Zhou, Y., Mu, Y., Loo, L.S., Cai, L., Thompson, R.C., Yang, B., et al. (2013). Loss of sorting nexin 27 contributes to excitatory synaptic dysfunction by modulating glutamate receptor recycling in Down's syndrome. Nat. Med. *19*, 473–480.

Wang, Y., Shi, G., Miller, D.J., Wang, Y., Broussard, G., Wang, Y., Tian, L., and Yu, G. (2016). FASP: a machine learning approach to functional astrocyte phenotyping from time-lapse calcium imaging data. In 2016 IEEE 13th International Symposium on Biomedical Imaging (ISBI), Prague, 2016 (IEEE), pp. 351–354.

Weick, J.P., Held, D.L., Bonadurer, G.F., 3rd, Doers, M.E., Liu, Y., Maguire, C., Clark, A., Knackert, J.A., Molinarolo, K., Musser, M., et al. (2013). Deficits in human trisomy 21 iPSCs and neurons. Proc. Natl. Acad. Sci. USA *110*, 9962–9967.

Wolosker, H., Balu, D.T., and Coyle, J.T. (2016). The rise and fall of the d-serine-mediated gliotransmission hypothesis. Trends Neurosci. *39*, 712–721.

Wolvetang, E.J., Wilson, T.J., Sanij, E., Busciglio, J., Hatzistavrou, T., Seth, A., Hertzog, P.J., and Kola, I. (2003). ETS2 overexpression in transgenic models and in Down syndrome predisposes to apoptosis via the p53 pathway. Hum. Mol. Genet. *12*, 247–255.

Zhang, S.C., Wernig, M., Duncan, I.D., Brüstle, O., and Thomson, J.A. (2001). In vitro differentiation of transplantable neural precursors from human embryonic stem cells. Nat. Biotechnol. *19*, 1129–1133.

Zhang, Y., Sloan, S.A., Clarke, L.E., Caneda, C., Plaza, C.A., Blumenthal, P.D., Vogel, H., Steinberg, G.K., Edwards, M.S.B., Li, G., et al. (2016). Purification and characterization of progenitor and mature human astrocytes reveals transcriptional and functional differences with mouse. Neuron *89*, 37–53.

Cell Reports, Volume *24*

Supplemental Information

Aberrant Calcium Signaling in Astrocytes Inhibits Neuronal Excitability in a Human Down Syndrome Stem Cell Model

Grace O. Mizuno, Yinxue Wang, Guilai Shi, Yizhi Wang, Junqing Sun, Stelios Papadopoulos, Gerard J. Broussard, Elizabeth K. Unger, Wenbin Deng, Jason Weick, Anita Bhattacharyya, Chao-Yin Chen, Guoqiang Yu, Loren L. Looger, and Lin Tian

Supplementary Information

1. Supplementary Figures

A

Cell line identifier	Karyotype	Source fibroblasts	Reprogramming method
DS2U	Euploid	AG05397, male, 1 year	Retrovirus
DS1	Ts21	AG05397	Retrovirus
DS4	Ts21	AG05397	Retrovirus

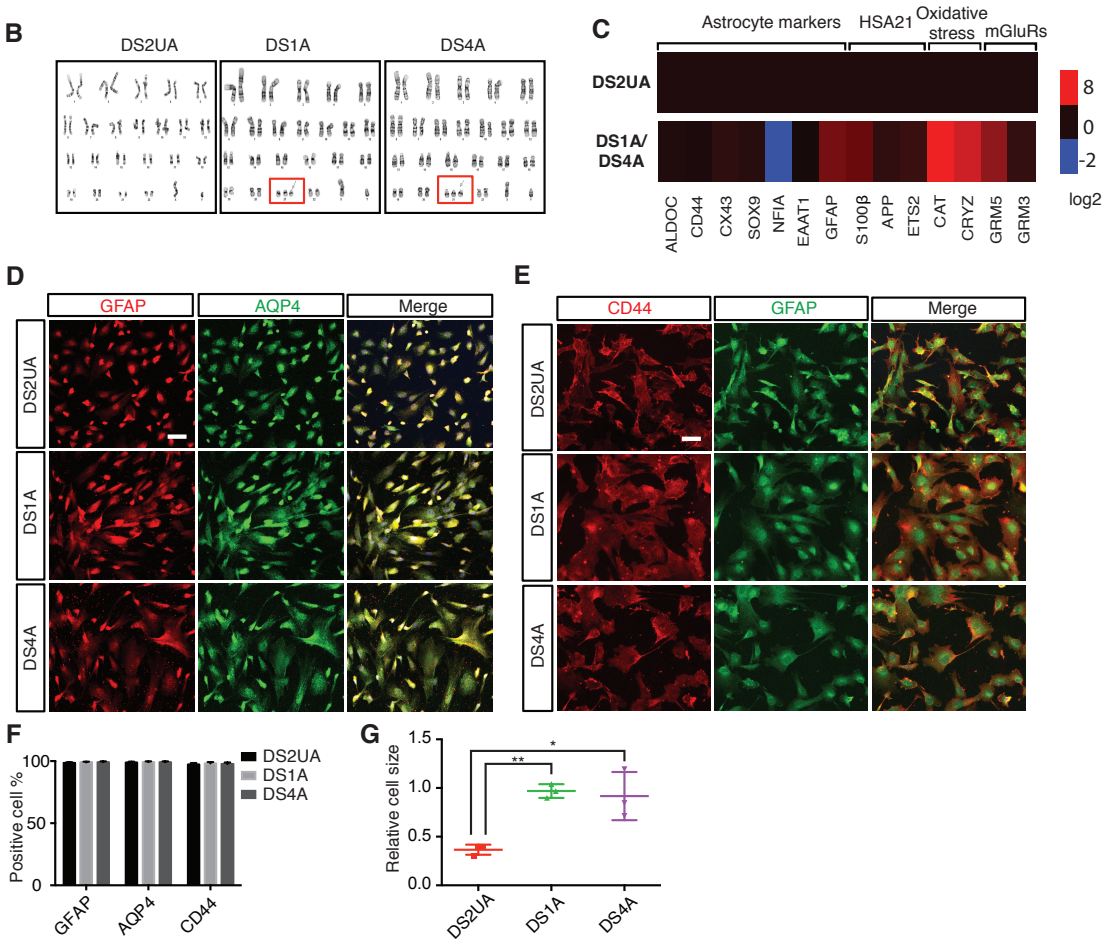

Figure S1. Differentiation and characterization of human iPSC-derived astroglia. Related to Figure 1. (a) Table of differentiated lines used in this study. (b) Karyotype analysis of human iPSC-derived astroglia and primary astrocytes (HA). Trisomy of HSA21 indicated with red boxes. (c) qPCR analysis of astrocytic markers, genes on HSA21, or genes associated with oxidative stress in iPSC-derived astroglia. The expression levels of genes in DS astroglia (DS1A and DS4A) were normalized to levels in isogenic DS2UA. (d-f) Astrocyte markers, such as GFAP, AQP4 and CD44, were broadly expressed in human iPSC-derived astroglia. Co-immunostaining of GFAP with AQP4 (d) or CD44 (e) and quantitation (f) are shown. Scale bar: 50 μm. (g) Relative cell sizes of iPSC-derived astroglia.

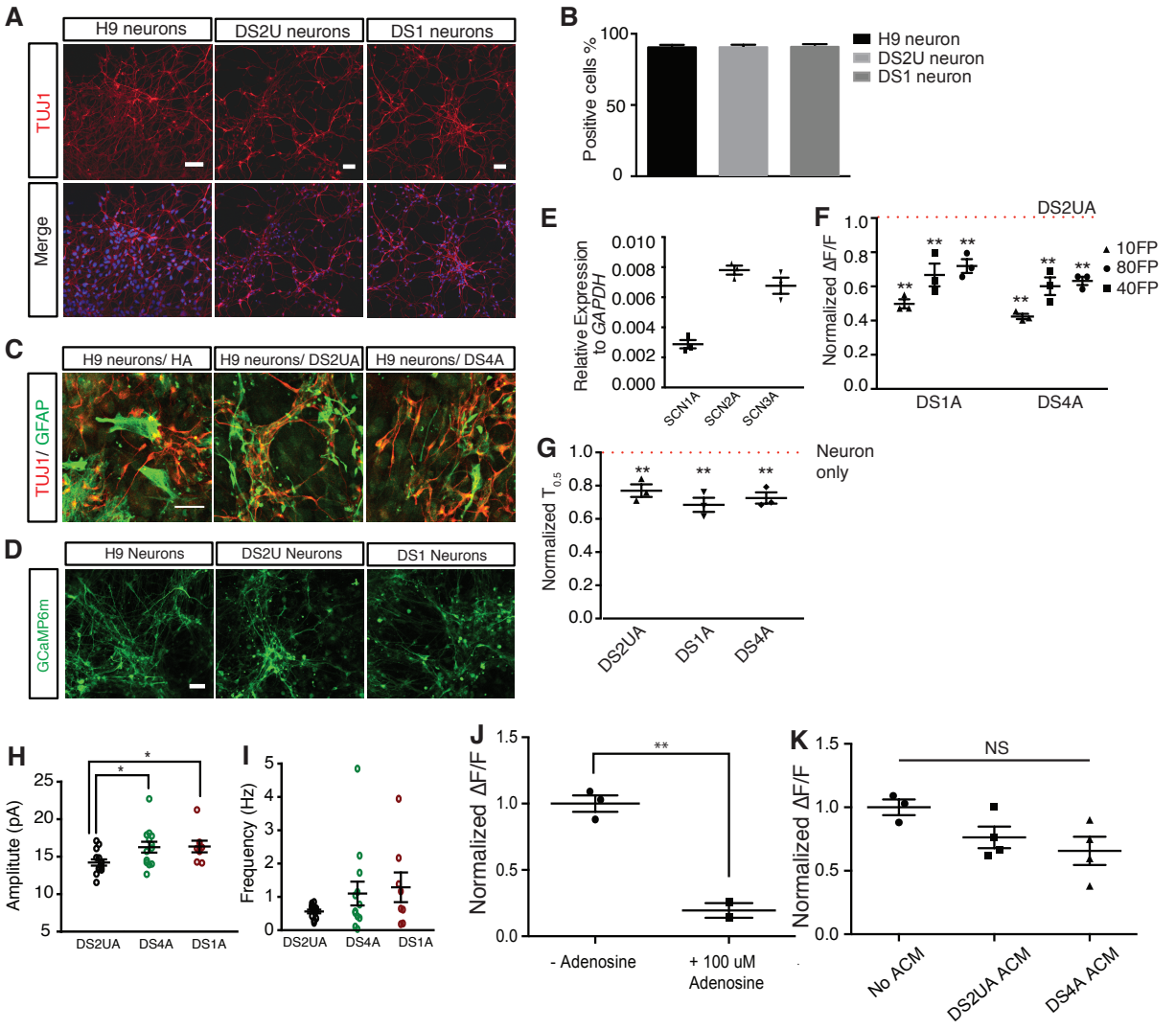

Figure S2. Characterization of ESC or iPSC-derived neurons. Related to Figure 1. (a) Expression of TUJ1 in H9 hESC, isogenic DS2U and DS1 iPSC-derived neurons. (b) Percentage of neurons showing expression of TUJ1. (*n*=3 images of immunostaining) (c) Expression of TUJ1 and GFAP in H9-neurons co-cultured with control HA, isogenic control DS2UA and DS1A. (d) Expression of GCaMP6m in H9 hESC, isogenic DS2UA and DS1 iPSC-derived neurons. (e) Real-time qPCR analysis of the expression of voltage gated sodium channels in H9 hESC-derived neurons, normalized to GAPDH (*n*=3). (f) ΔF/F of H9 hESC-derived neurons in response to a variety of FPs when co-cultured with DS1A or DS4A. ΔF/F was normalized to that when co-cultured with DS2UA (red dotted line). (g) Response kinetics of H9 hESC-derived neurons to 40 FPs, when co-cultured with DS2UA, DS1A or DS4A normalized to that of neurons alone (red dotted line) (*n*=3) (h) The mean amplitude was significantly higher in DS4A and DS1A compared to the DS2UA group (Fisher's LSD test, $p<0.05$). (i) Although there was a trend for higher mEPSC frequencies in the DS4A and DS1A groups, the differences were not statistical significant. (j-k) Suppressed neuronal activity is influenced by purinergic signaling. (j) H9-neurons incubated with 100 µm adenosine resulted in suppressed neuronal activity (normalized ΔF/F of 100 µM adenosine (*n*=2) to without adenosine (*n*=3) =0.20±0.06, *P*=0.0032). (k) H9-neurons incubated with DS4A or DS4A ACM trended towards suppressed neuronal activity (ACM from DS4A suppressed neuronal excitability by 0.34-fold versus 0.24-fold from DS2UA ACM normalized to no ACM (*n*=3), *P*=0.06 DS4A (*n*=4), *P*=0.091 DS2UA (*n*=4)).

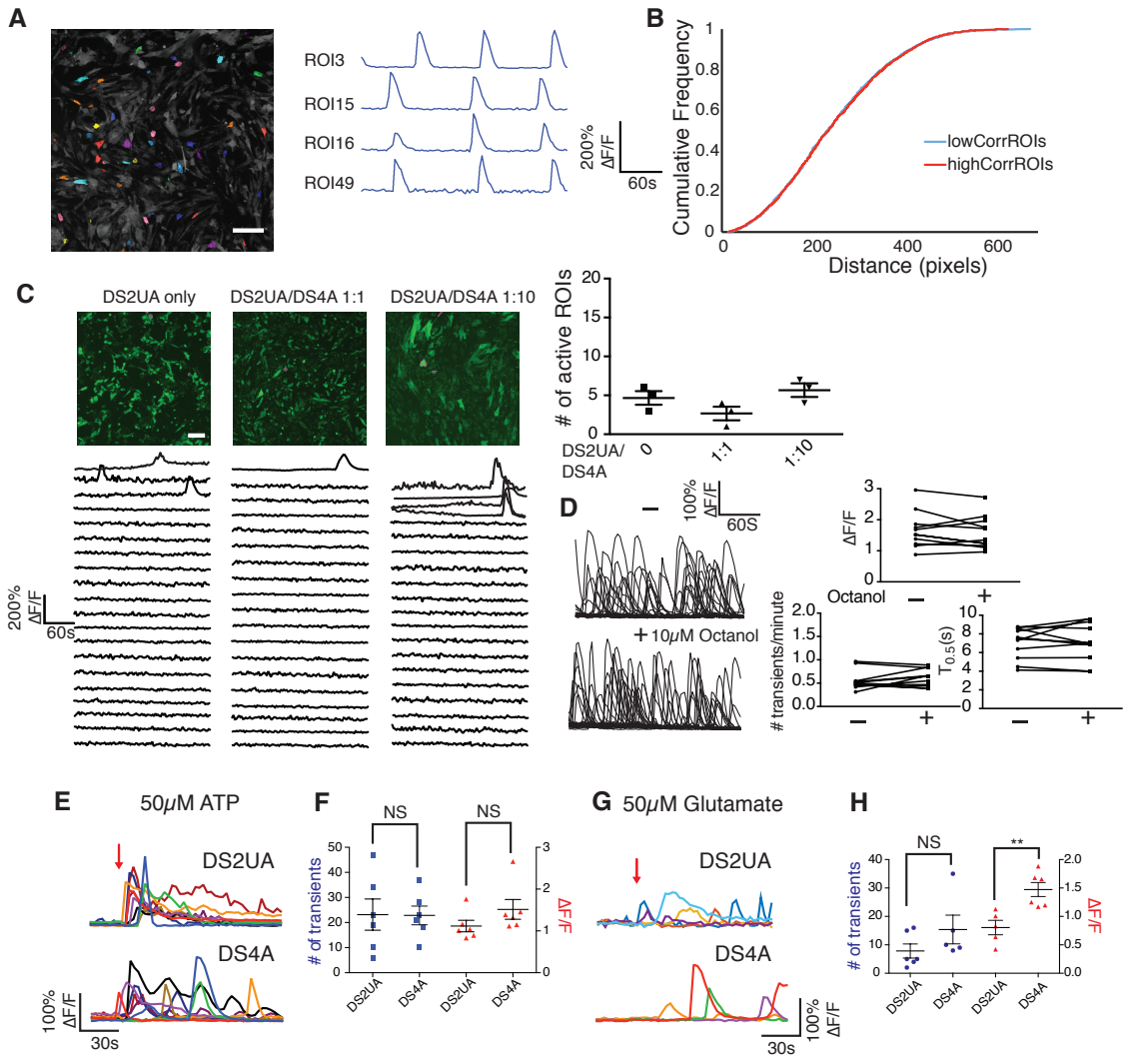

Figure S3. Fluctuation dynamics and Ca^{2+} fluctuations in isogenic and DS astroglia. Related to Figure 2. (a-d) Spontaneous calcium could not be induced in isogenic astroglia when co-cultured with DS astroglia. (a-b) Analysis of Ca^{2+} transients revealed 33 clusters of cells (n=93) in DS4A with correlated temporal dynamics (a), while their locations were randomly distributed (b). Each cluster was labeled with a specific color, and Ca^{2+} traces from one representative cluster in 5 min is shown. Scale bar: 200 μm (a). Temporally correlated ROIs showed similar spatial distribution with randomly selected ROIs that were not correlated in temporal dynamics. (c) The number of active ROIs (3 imaging sessions of 5 min) in DS2UA alone or in the presence of co-cultured DS4A at different ratios. Ca^{2+} traces from 20 ROIs are also shown. (d) The gap junction blocker octanol failed to modulate the properties of spontaneous Ca^{2+} fluctuations in DS4A. Representative traces of Ca^{2+} fluctuations (n=11) without treatment and in the presence of 10μM octanol. Quantification of the amplitude, frequency and $T_{0.5}$ of these Ca^{2+} fluctuations before and after treatment. Scale bar: 100 μm. (e-h) Astroglia response to ATP and glutamate. Representative Ca^{2+} responses of control isogenic DS2UA and DS4A were shown in selected region of interests (10 ROIs for ATP (e) and 5 ROIs for glutamate (g)). Number of Ca^{2+} transients in 150 s with addition of 50 μM ATP and their averaged ΔF/F (f) from at least 3 independent imaging sessions. Number of Ca^{2+} transients in 150 s, with addition of 50 μM glutamate and their averaged ΔF/F (h).

A

Gene group	Genes
mGluRs	GRM1/2/3/4/5/6/7/8
Purinergic receptors	P2RY1, ADORA1, ADORA2A, ADORA2B, ADORA3
GPCR pathway	GNAQ, SHANK1/2/3
ER Ca^{2+}	$IP_3R1/2/3$, RYR1/2/3, ATP2A1
Mitochondrial Ca^{2+}	NCLX, MCU
Plasma membrane Ca^{2+}	STIM1, ORAI1/2/3, NCX1/2/3, ATP2B1, TRPA1
Astroglial markers	S100β, SOX9, FABP7, NF1A, EAAT1/2, CX43, AQP4, ALDOC, CD44

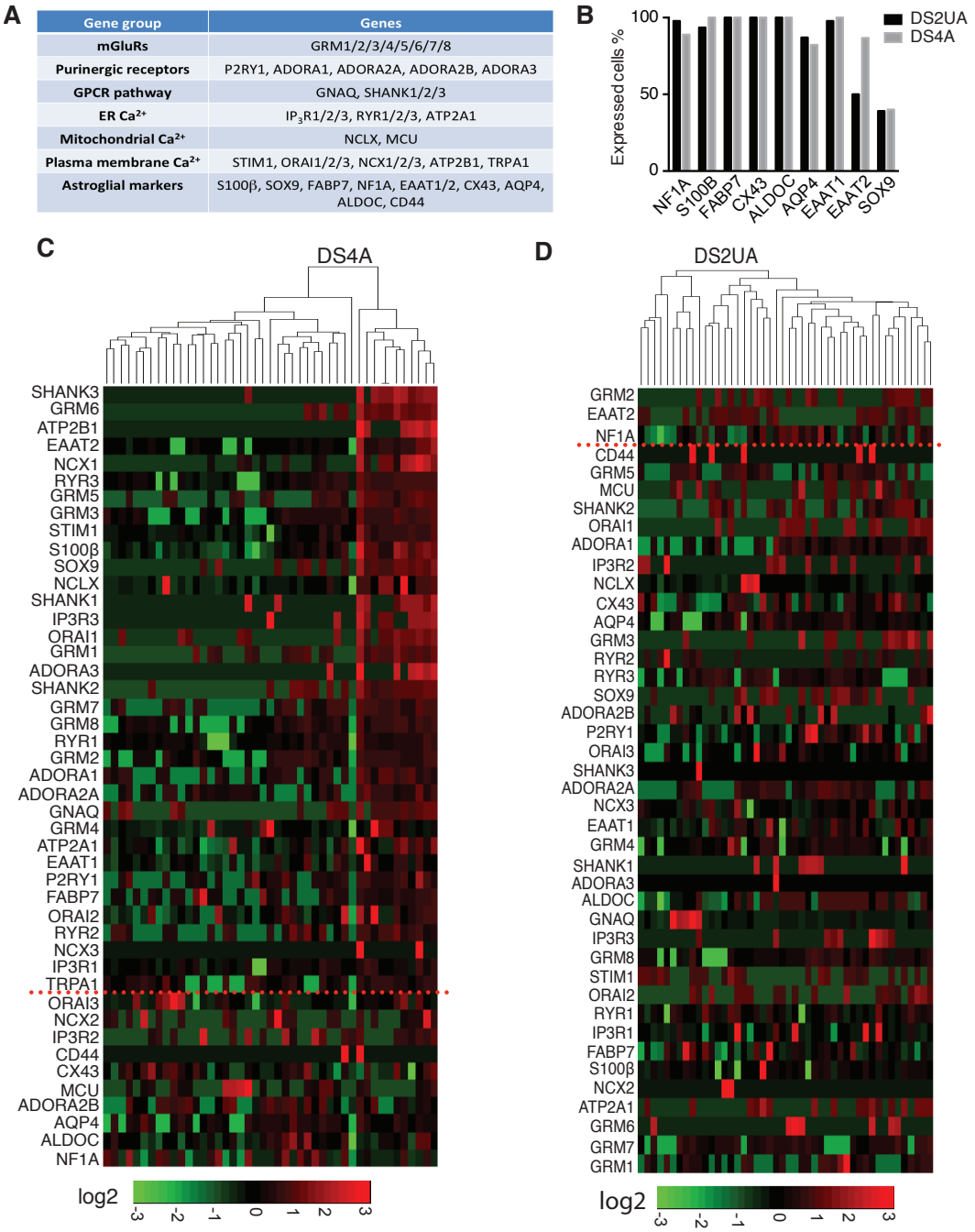

Figure S4. Single-cell gene expression analysis of human iPSC-derived astroglia. Related to Figure 4 and Figure 5. (a) Table of selectively analyzed gene transcripts encoding Ca^{2+} handling toolkits as well as cell-type specific markers. (b) Percentage of cells expressing a given cell-specific markers (n=46 for DS2UA and 45 for DS4A). (c-d) Heatmaps showing the expression of gene transcripts encoding astroglial markers and Ca^{2+} handing toolkits, including mGluRs, purinergic receptors and intracellular Ca^{2+} pathways, in individual cells of DS4A (c) and DS2UA (d). Each row represents a single astroglia. Dendrograms show unsupervised clustering based on differentially expressed genes. Genes are listed from top to bottom showing greatest to least differences between the two clusters (unsupervised clustering analysis). Red line shows threshold of $P<(0.05)$.

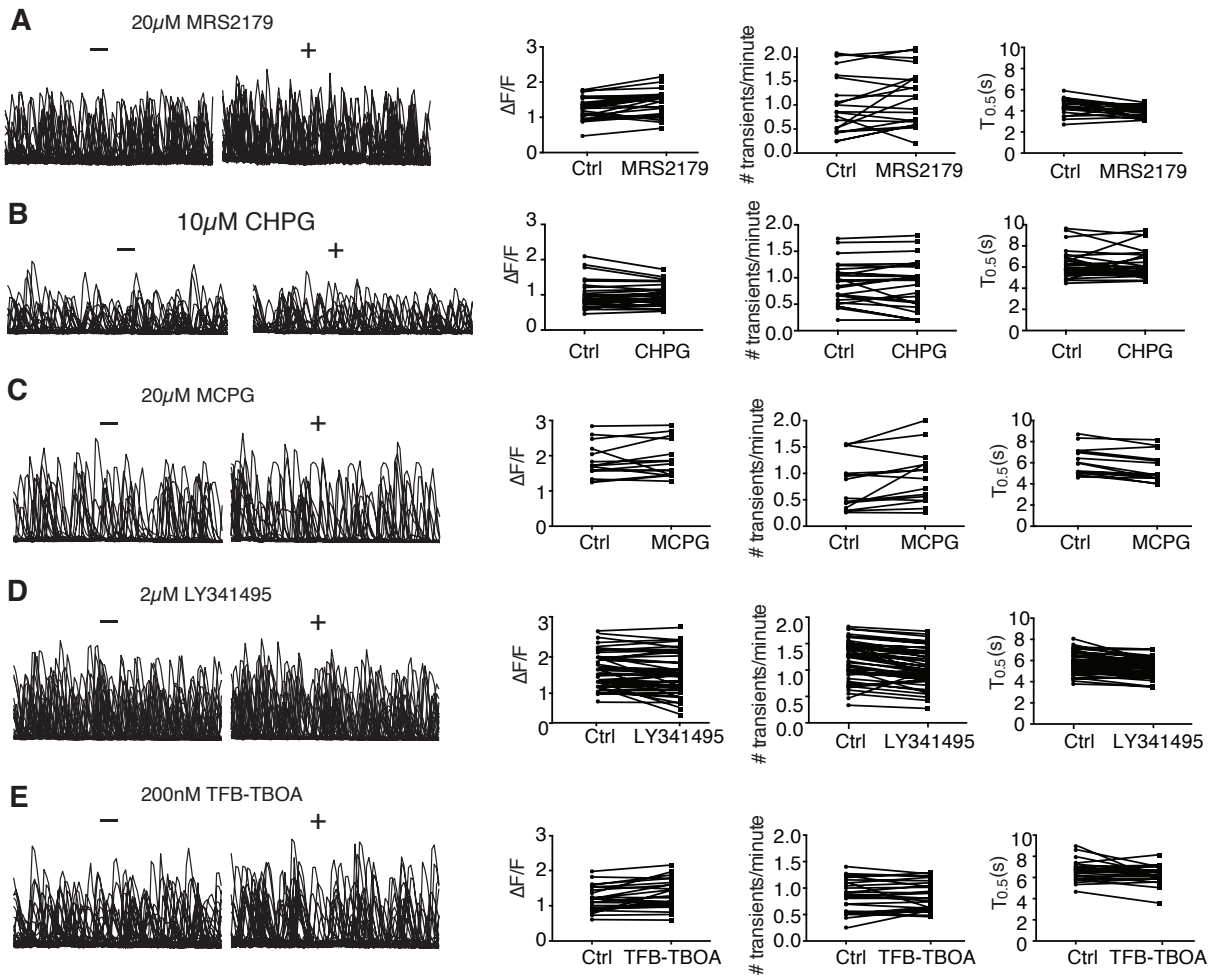

Figure S5. The effect of antagonists on Ca^{2+} fluctuations in DS4A. Related to Figure 4. Representative traces of Ca^{2+} fluctuations in the absence and presence of antagonists including mGluR5 agonist CHPG (30 ROIs, a) MRS2179 (24 ROIs, b), MCPG (15 ROIs, c), LY341495 (53 ROIs, d), and TFB-TBOA (28 ROIs, e). The amplitude, frequency and $T_{0.5}$ of these Ca2+ fluctuations before and after treatment are also shown.

2. Table S1. Gene and protein abbreviations

ALDOC	Aldolase, fructose-bisphosphate C
APP	Amyloid beta precursor protein
AQP4	Aquaporin 4
ATP2B1	ATPase plasma membrane Ca^{2+} transporting 1
CAT	Catalase
CD44	CD44 cell adhesion molecule
CRYZ	Crystallin zeta
CX43	Connexin 43
DSCAM	Down syndrome cell adhesion molecule
DYRK1A	Dual specificity tyrosine phosphorylation regulated
EAAT1	Excitatory amino acid transporter 1
EAAT2	Excitatory amino acid transporter 2
ETS2	ETS proto-oncogene 2, transcription factor
GFAP	Glial fibrillary acidic protein
IP3R3	Inositol 1, 4, 5-triphosphate receptor type 3
KCNJ6	Potassium voltage-gated channel subfamily J member 6
mGluRs	Metabotropic glutamate receptors (GRM3, GRM5)
miR-155	MicroRNA 155
NCLX	Sodium/ potassium/ calcium exchanger
NCX1	Sodium/ calcium exchanger
NF1A	Nuclear factor I A
NKCC1	Sodium potassium chloride transporter
ORAI	Calcium release activated calcium channel protein
P2R	Purinergic receptors
RYR1/3	Ryanodine receptor
S100β	S-100 calcium-binding protein subunit β
SIM2	Single-minded transcription factor 2
SOX9	Protein critical for embryonic development
STIM	Stromal interaction molecules

3. Supplementary Materials and Methods

Lentivirus production

Lentiviruses were produced by co-transfecting HEK293T cells (ATCC) with 5 μg pSIV-*Synapsin-1*-GCaMP6m or pHIV-*EF1α*-Lck-GCaMP6m, scrambled or S100β shRNAs, 2 μg pHCMV-G, and 3 μg pCMV-deltaR8.2, using 40 μl SuperFect (Qiagen, 301305). Supernatant containing viral particles was collected, filtered, and concentrated 72 h later with an Ultra-4 centrifugal filter (Millipore, UFC810024).

mEPSC recordings and analysis

Whole-cell voltage clamp experiments were performed 17–19 days after plating. mEPSCs were recorded in an external solution containing 140 mM NaCl, 5 mM KCl, 10 mM HEPES, 2 mM CaCl2, 1 mM MgSO4, 1 μM tetrodotoxin (TTX), 50 μM AP-5, and 20 μM bicuculline (pH 7.4 with NaOH, 290 mOsm/l). Borosilicate glass electrodes were filled with an internal solution containing 145 mM CsCl, 1 mM EGTA, 5 mM HEPES, 0.1 mM CaCl2, 2 mM MgSO4 (PH 7.4 with CsOH, 275 mOsm/l). The seal resistance was greater than 1 GΩ and the series resistance was no greater than 20 MΩ. All recordings were made with an Axopatch 200B patch-clamp amplifier (Axon Instruments, Foster City, CA, USA). Whole-cell currents were filtered at 2 kHz and digitized at 10 kHz. All neurons were voltage-clamped at –60 mV. The mEPSC events were detected with Mini Analysis software (Synaptosoft Inc., Fort Lee, NJ, USA). The accuracy of detection was confirmed by visual inspection.

Immuncytochemistry

Cells maintained on cover glasses (Fisher Scientific, 12-545-81) were washed with PBS 3 times before being fixed with 4% paraformaldehyde (VWR, 100503-916) for 15 min. After washing, cells were treated with 0.1% Triton X-100 (Fisher Scientific, BP151-500) for 10 min, blocked

with 10% bovine serum albumin (Sigma, A9647) for 60 min, and incubated with primary antibodies at 4 °C overnight followed by secondary antibodies for 1 h at room temperature. Cells were washed with PBS 2 times after each antibody incubation and mounted on glass slides (Fisher Scientific, 12-550-123) using ProLong® Gold Anti-fade Mountant with DAPI (Thermo Fisher Scientific, P36935). Primary antibodies used included: AQP4 (Santa Cruz Biotech, sc-20812, rabbit), CD44 (Abcam, ab6124, mouse), GFAP (Millipore, MAB360, mouse; AB5840, rabbit), TUJ1 (COVANCE, MMS-435P, mouse), Synapsin-I (Millipore, AB1543, rabbit), S100 β (Abcam, ab11178, mouse), and PSD95 (NeuroMab, K28/43, mouse). Secondary antibodies included Alexa488-conjugated donkey anti-rabbit (A21206) and Alexa594-conjugated goat anti-mouse (A11005), and were purchased from Thermo Fisher Scientific.

Immunocytochemistry analysis

Images were obtained using a Zeiss LSM 710 confocal microscope (× 40 magnification, N.A. 1.3 oil objective). All immunostaining experiments were performed 3 times, and representative results were presented.

Puncta density quantification: Using the spot-detection feature in the Imaris software (Bitplane) the number of colocalized Synapsin-1 and PSD95 per μm of dendrite was obtained to calculate the puncta density. S100 β immunocytochemistry analysis: Using FIJI the fluorescence intensity of each imaging field was analyzed.

Ca^{2+} imaging analysis of astrocytes using FASP

As an unsupervised analytic method, FASP is data-driven, learning model parameters using machine-learning techniques to automatically detect ROIs displaying Ca^{2+} fluctuation. In addition, designed under probabilistic principles, FASP has strong statistical power to detect

weak signals (ROIs) that are easily ignored by purely manual analysis. Our simulation study verified that some ROIs with weak signals were ignored by manual analysis but correctly detected by FASP. By judicious application of various statistical theories, FASP confers tuning parameters with probabilistic meaning, which can be directly translated into the false discovery rates. This algorithm greatly facilitates the usability of parameter settings and ensures the reproducibility of the results and equal comparison across experiments.

Specifically, we set a single threshold corresponding to a false discovery rate of 0.01; that is, an average of 1% of all identified active ROIs are expected to be false positives. The threshold is fixed for all experiments and conditions.

Given a time-lapse astrocytic Ca^{2+}-imaging data set, FASP generates a set of ROIs and corresponding characteristic curves. For each pixel in an ROI, there is a corresponding activity curve for which the time shift with respect to the characteristic curve is also estimated. Based on the results of FASP, we quantified various parameters of astrocytic Ca^{2+} signals according to the following:

- The signal-to-baseline ratio of fluorescence was calculated as

$$\frac{\Delta F}{F_0} = \frac{F - F_0}{F_0},$$

  where the baseline fluorescence F_0 is estimated as the 10^{th} percentile of the fluorescence level over all time points of the measurement.
- The number of Ca^{2+} transients is calculated as the number of peak responses from all ROIs detected in each time-lapse imaging session.
- The number of active ROIs is calculated as the total number of ROIs detected by FASP in the field of view of each time-lapse imaging session.

Amplitude: To calculate the amplitude of a Ca^{2+} transient we first transformed the raw time-intensity curves into signal-to-baseline ratio of fluorescence ($\Delta F/F0=(F-F0)/F0$), where the baseline fluorescence F0 is estimated as the 10^{th} percentile of the fluorescence levels (intensities) at all the time points during measurement.

Frequency: To calculate the frequency of Ca^{2+} fluctuations more reliably, we first determined the average duration between 2 contiguous events, and then defined the frequency as the inverse of the average duration. For those ROIs that only displayed single Ca^{2+} transients during the imaging session, the information contained in the single-event time series is insufficient for point estimation of frequency. These ROIs are expected to have a positive frequency between 0 and 0.2 transients per minute.

$T_{0.5}$: Decay kinetics or $T_{0.5}$(off) was calculated using linear interpolation as the time from peak to half-amplitude of an event.

Propagation speed wavefront analysis: On the basis of estimated pixel-wise time shifts from the characteristic curve, wavefronts of Ca^{2+} transients were located; accordingly, the propagation speed of Ca^{2+} events within an ROI was obtained by estimating the average distance between wavefronts. Active ROIs detected in DS4A were divided into 33 clusters of timed coincidence by unsupervised clustering analysis (Affinity Propagation Clustering Algorithm)[57]. Any pairs of ROIs within the same cluster were recognized as highly coincident, while any pairs of ROIs from 2 different clusters were recognized as weakly coincident. Distributions of pixel distance of correlated and uncorrelated pairs were then measured and plotted.

Neuron-astrocyte co-culture or astrocyte conditioned media imaging

All neuronal imaging experiments were repeated 3 times, and 10 ROIs were selected for analysis using a customized script (FluoAnalyzer) in MATLAB (MathWorks). ROIs (*n*>10 for each imaging file) were manually selected, and the fluorescence intensity (F) at each frame was quantified as the mean of all selected ROIs. The neuronal responses were calculated as ΔF/F ($F-F_0/F_0$), where F was quantified as the mean of all selected ROIs (*n*>10 in each field of view), and F_0 was taken as the mean of all ROIs across the first 3 frames.

RNA isolation and qPCR

Total RNA was prepared from cells *(n*=3) with RNeasy kit (Qiagen, 74104). Complementary DNA was prepared with iScript RT Supermix (Bio-Rad, 170-8841). qPCR was performed with iTaq™ Universal SYBR® Green Supermix (Bio-Rad, 172-5121) on a CFX96™ Real-Time System (Bio-Rad), and the data was collected with Bio-Rad CFX Manager 3.0. Gene expression levels were quantified relative to the housekeeping gene, *GAPDH*.

Single-cell expression analysis

The values of gene expression were pre-processed by taking the inverse, applying a square-root transformation, and rescaling the expression to zero mean and unit variance. The similarity matrix was computed first using the default method of negative distance (default parameters), and affinity propagation clustering was applied by setting the desired number of clusters to 2 in the R package, Apcluster.

The single-cell expression analysis consisted of 4 major components as detailed below:

Preprocessing: In the raw data, the value for each gene denotes how many amplification

cycles were required to cross the threshold, which is set using the AutoGlobal method. In our data, the maximum observed value was 29. A missing value indicated that the corresponding gene had too little expression to be amplified to reach the threshold quantity. In the raw data, missing values were marked by 999. We replaced all missing values by 60, which was around 2 times the maximum value observed. Then, the inverse of the values was used to represent the amount of expression. A square-root transformation was applied to each gene to normalize for expression-level differences. Finally, for each cell, all genes were normalized to have zero mean and unit variance to highlight differences between cells.

Clustering analysis: Affinity propagation clustering (APC) was applied. The algorithm was implemented in the R package, Apcluster. The algorithm requires users to input a similarity matrix. The default settings were adopted; in other words, Euclidian distance was calculated based on the data matrix and the negative distance was used as the similarity matrix. To be consistent with the observation that there were 2 groups of astrocytes, one with active Ca^{2+} fluctuations and the other one without, the desired number of clusters was set to 2. Notably, we did not know which cells were active, and the analysis was unsupervised.

Assessing statistical significance of resultant clusters: Since a clustering algorithm can always generate clusters even if there are no clusters actually present in the data, we sought to evaluate whether the resultant clusters were purely by chance. The null hypothesis was that there were no groups of cells that were closer within-group than between-groups (i.e., distances between cells were uniformly distributed). Permutation was used to generate the distribution for the null hypothesis. All genes in the data set were permuted 100,000 times, resulting in 100,000 data sets following the null hypothesis. For each resulting data set, we ran APC to get 2 groups. In APC, the objective function was the overall similarity. A histogram was obtained based on the

100,000 overall similarities. The position of the observed overall similarity indicated the significance of the observed value.

Differentially expressed genes between clusters: Standard differential analysis, such as t-test between groups, cannot be applied here because the clustering was based on all genes; hence, each gene was biased toward differential expression between clusters. To correct for this bias, a permutation procedure was designed. To test the significance for each gene, we shuffled the values in that gene 10,000 times while keeping all other genes fixed. In this way, the gene would not interfere with the clustering results, so there would be no bias. Each time we ran the clustering algorithm APC to get 2 groups. Based on the new clustering results, the significance of the gene was recorded and summarized into a histogram, which could be further used to derive the corrected *P* value. For example, if the original *P* value was 0.01, corresponding to the 2^{nd} percentile in the histogram, the corrected *P* value would be 0.02.

Fluorescence-activated cell sorting (FACS)

DS astrocytes were infected with lentiviruses expressing S100β-shRNA-mCherry and collected 3 days later for sorting, which was performed by the FACS core at UC Davis. The top 15% of cells expressing high amounts of mCherry measured on fluorescence intensity were collected as mCherry “high”, and the bottom 18% of cells expressing low amounts of mCherry were collected as “low”. High mCherry fluorescence represents high expression of S100β shRNA and less expression of S100β.

Inhibiting extracellular S100β

S100β (Abcam, ab11178) and TUJ1 (COVANCE, MMS-435P) antibodies (diluted 1:1000) were used to pretreat DS astrocytes for 10 minutes before imaging.